THESIS

KEMITEKNIK
HÖGSKOLEINGENJÖRSUTBILDNINGEN

Chemical analysis for mapping of soot reactivity

Henrik Pettersson

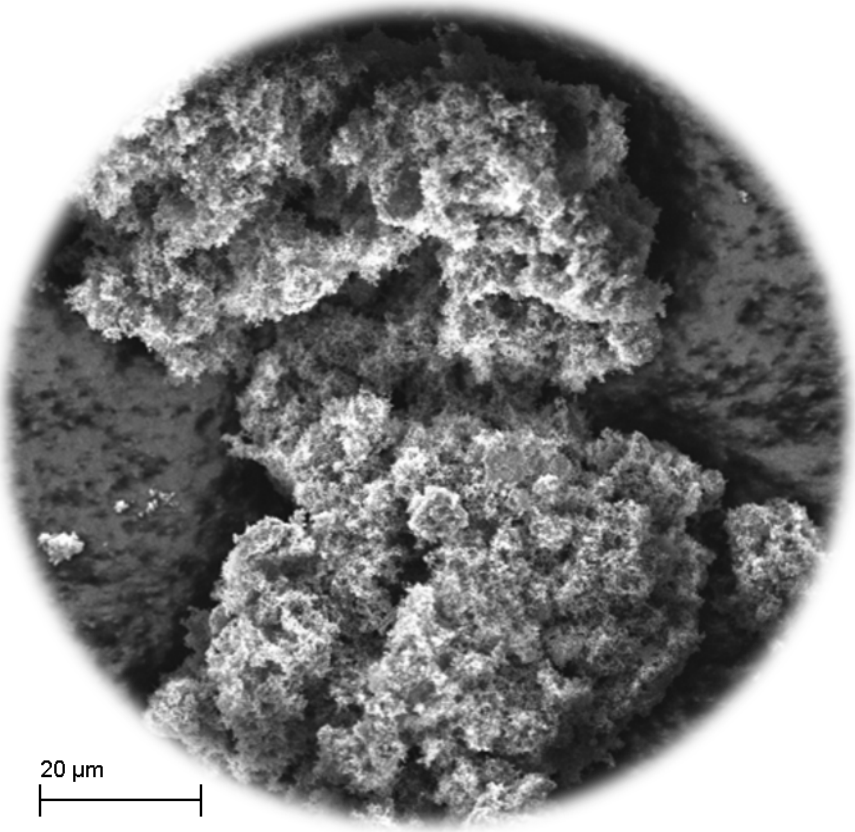

KTH
Stockholm
2013

KTH KEMITEKNIK
HÖGSKOLEINGENJÖRSUTBILDNINGEN

THESIS

TITLE:	Chemical analysis for mapping of soot reactivity
SWEDISH TITLE:	Kemisk analys för kartläggning av sots reaktivitet
KEYWORDS:	diesel soot, reactivity, oxidation, rail pressure, EGR, TGA, SEM, EDS
WORKPLACE:	Scania CV AB
SUPERVISOR AT WORKPLACE:	Marita Nilsson
SUPERVISOR AT KTH:	Lars J. Pettersson
STUDENT:	Henrik Pettersson
DATE:	
APPROVED:	
EXAMINER:	Lars J. Pettersson

Abstract

In order to increase the efficiency of diesel particulate filter regeneration more knowledge about diesel soot and its reactivity is required. This thesis compares soot created during accelerated filter loading by lowered rail pressure, with soot from normal filter loading. Soot properties and their correlations to oxidation reactivity are also examined through thermogravimetric analysis, scanning electron microscopy, energy dispersive x-ray spectroscopy, BET nitrogen sorption, and FTIR spectroscopy. The usefulness of these analysis methods was also evaluated. The soot samples consisted of two carbon blacks for reference (Printex U and Vulcan XC 72), four accelerated soot samples and two non-accelerated samples. The results showed that the accelerated samples contained less volatile organic compounds than the non-accelerated soot and required slightly higher temperatures to oxidize in air. Soot with a high oxygen/carbon ratio and high levels of volatile organic compounds was found to be the most reactive. The most useful method for analyzing the soot was the thermogravimetric analysis. The scanning electron microscopy and energy dispersive x-ray spectroscopy were useful additions but the FTIR spectroscopy provided very little useful information. The usefulness of BET nitrogen sorption was not decisively concluded.

Sammanfattning

För att kunna förbättra regenereringen av dieselpartikelfilter krävs en ökad kunskap om dieselsot och dess reaktivitet. I detta examensarbete jämförs sot som skapas vid accelererad sotinlagring genom sänkt railtryck, med sot från normal sotinlagring. Hur sotets egenskaper påverkar dess reaktivitet undersöks också genom termogravimetrisk analys, svepelektronmikroskopi, energidispersiv röntgenspektroskopi, BET-kväveadsorption och FTIR-spektroskopi. Hur väl dessa analysmetoder lämpar sig för analys av sot utvärderades också. Sotproverna utgjordes av två så kallade ”carbon black” för referens (Printex U och Vulcan XC 72), fyra accelererade sotprov och två icke-accelererade prov. Resultaten visade att de accelererade proverna innehöll mindre flyktiga organiska föreningar än icke-accelererade sot och krävde något högre temperaturer för att oxideras i luft. Sot med ett högt syre/kol-förhållande och höga nivåer av flyktiga organiska föreningar visade sig vara mest reaktivt. Den mest användbara metoden för att analysera sot var den termogravimetriska analysen. Svepelektronmikroskopi och energidispersiv röntgenspektroskopi var användbara som komplementerande metoder men FTIR-spektroskopi gav väldigt lite användbar information. Ingen konkret slutsats drogs gällande nyttan av BET-kväveadsorption.

Acknowledgements

This thesis was performed at Scania CV AB at the department for Engine Performance & Emissions (UTMC). I would like to thank everyone in UTMC for their support with special thanks to my supervisors Marita Nilsson and Hanna Lind for their guidance.

I would also like to thank Sara Alfredsson and Ali Saramat from UTMC for instructing me in the use of the scanning electron microscope and the FTIR spectrometer.

Thanks to Moa Ziethén Granlund, KTH, for her assistance with the BET analyses.

Finally I would like to thank my examiner Lars J. Pettersson, KTH, for his good advice and for procuring the Vulcan XC 72 sample.

Table of Contents

1 Introduction

The new Euro VI emission standard limits the particle matter emissions for heavy-duty diesel engines to 0.01 g/kWh and $8.0*10^{11}$ particles/kWh [1]. In order to meet these requirements vehicles are equipped with diesel particulate filters (DPFs), which capture the particulate matter from the exhaust stream. The main component of this particulate matter is soot, which can be combusted under the right circumstances. The reactivity of the soot depends heavily on the conditions under which it was formed and it is becoming increasingly important to understand the correlations between the engine's operating parameters, the chemical and physical structure of the soot and its oxidation reactivity. Increasing the knowledge about the soot will allow for more efficient regeneration of the particulate filter and thereby reduce the wear on the filter, lower the fuel consumption and minimize particulate emissions.

2 Objective

The primary objective of this thesis is to compare soot generated during accelerated DPF loading with soot produced from normal DPF loading and determine if the accelerated soot is representative of regular soot and can be used as a plausible surrogate in DPF regeneration testing. The secondary objective is to investigate what kind of soot is especially reactive. This will be done by formulating an Arrhenius type rate expression for the oxidation reaction and determining the kinetic parameters, e.g. the activation energy and the pre-exponential factor, through thermogravimetric analyses (TGA). The structure of the soot will also be examined using BET nitrogen sorption and scanning electron microscopy. Energy dispersive x-ray spectroscopy (EDS) will be used to determine the carbon/oxygen ratio in the soot samples and Fourier transform infrared (FTIR) spectroscopy will provide information about the functional groups on the soot's surface. The relative importance of these analyses, as methods for determining the reactivity of soot samples, will also be discussed.

3 Background

3.1 Diesel PM/Soot

Diesel particulate matter (PM) is a complex emission with many different components. An example of PM composition is shown in Figure 1. These components are generally separated into three groups: the solid fraction, the soluble organic fraction and sulfate particulates.

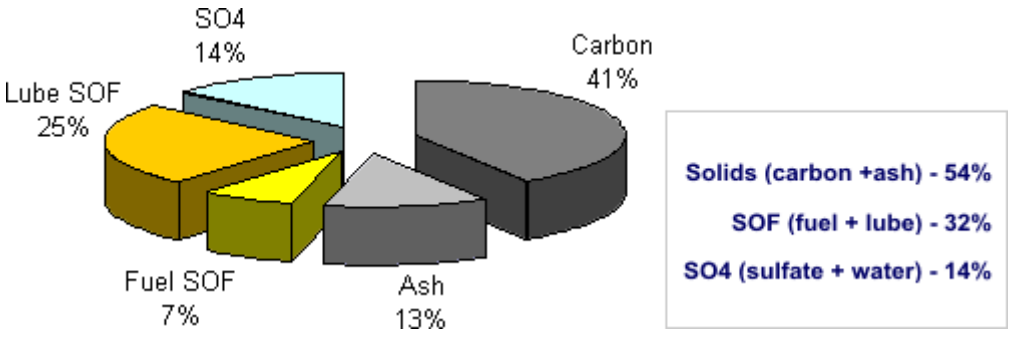

Figure 1. Composition of diesel particulate matter from a post-1994 US heavy-duty diesel engine [2]

The solid fraction usually makes up the largest part of the PM and is primarily composed of elemental carbon and ash. The elemental carbon in the PM is commonly referred to as soot and it is produced as a result of the heterogeneous nature of the diesel combustion. When the air/fuel mixture is too rich in fuel the combustion of the diesel is incomplete and it is this partial combustion that results in the forming of soot. The ash is generally made up of sulfates, phosphates or various metal oxides that are formed when the additives present in the lube oil are burned in the engine. It can also contain metal oxides that have resulted from wear on the engine or exhaust system.

The soluble organic fraction (SOF) consists of heavy hydrocarbons derived from unburned diesel fuel or the engine's lubricating oil. These hydrocarbons are also a product of the heterogeneous mixture of fuel and air but from areas with a lean fuel mixture. These mixtures do not burn properly and result in unburned hydrocarbons which are adsorbed on the surface of the carbon particles that make up the soot.

The sulfate particulates are formed when sulfur from the fuel is oxidized and then reacts with water to form sulfuric acid. The sulfuric acid subsequently goes through a heteronucleation process with water to form the sulfate particulates. [2-4]

3.2 DPF

In order to capture the diesel particulate matter, and keep it from being released into the atmosphere, diesel particulate filters (DPFs) are used in modern diesel vehicles. These DPFs are devices that physically remove the PM from the exhaust gases through filtration. They are most effective at filtering the solid components (the soot and ash) in the PM, with a filtering efficiency in the range of 95-99.9% by weight. The DPFs are however less effective at filtering the non-solid components of the PM (SOF and sulfate particulates).

DPFs are usually constructed from porous ceramic materials in a structure with many parallel channels which are alternatively blocked in one end. This design is called a wall-flow monolith and as Figure 2 illustrates, it forces the gas to flow through the filter walls.

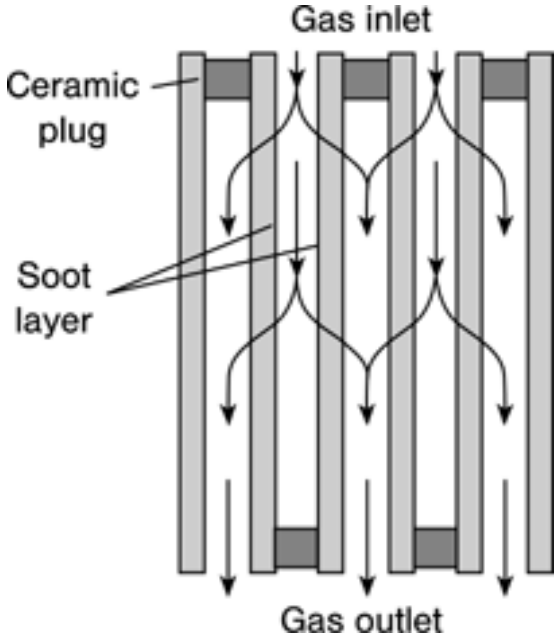

Figure 2. Gas flow in a wall-flow monolith particulate filter [5]

At the start when the DPF is empty, the filtration works primarily through a mechanism known as deep-bed filtration where the soot enters the porous material of the channel walls and is captured within its pores. As more soot is collected in the filter a soot cake is formed on the surface of the channel walls. This cake increases the filtration efficiency through a sieving process but as the soot cake grows and the filter becomes loaded with PM the gas flow gets obstructed and causes a pressure drop across the DPF. This pressure drop decreases the engine's performance and can increase the fuel consumption. To prevent the filter from becoming overloaded and blocked the DPF needs to be regenerated regularly by oxidation of the soot. [5-6]

3.2.1 Regeneration

Regeneration of the DPF can occur by soot oxidation with oxygen or nitrogen dioxide. Oxygen based regeneration has the advantage that diesel exhaust fumes practically always contain sufficient amounts of oxygen for the reaction to take place. The drawback is however that very high temperatures, typically above 600°C, are required in order to achieve decent reaction rates. For this reason, regeneration with oxygen is mostly used in active DPF systems where the exhaust temperatures are temporarily increased by management of the engine or by injecting some extra fuel directly into the exhaust upstream from a diesel oxidation catalyst (DOC), which generates heat by oxidizing the fuel. This procedure must be repeated regularly to prevent the filter from becoming overloaded. If too much soot is loaded into the filter there is a risk that the temperature can spike locally when it oxidizes and cause damage to the filter itself. The ignition temperature of the soot can be lowered slightly by introducing a catalyst as a coating on the filter or as an additive in the fuel.

The soot can also be oxidized by nitrogen dioxide (NO_2). This oxidation reaction occurs at temperatures as low as 250°C and can thus regenerate the DPF continuously. While this reaction does not require the same high temperature as the oxidation by oxygen, a higher concentration of NO_2 than is normally present in diesel exhaust is necessary. It can however be formed by oxidizing the nitric oxide (NO) from the exhaust with an oxidation catalyst placed upstream from the filter or alternatively, as a coating on the filter itself. Combinations of active regeneration and continuous or "passive" regeneration can also be used to ensure a proper regeneration of the DPF. [5-7]

3.3 Previous research

Several studies have been conducted in order to better comprehend the correlations between the reactivity of diesel soot and its physical structure, chemical composition, what fuel it was produced from and how the engine was operated.

3.3.1 Reaction rate

The oxidation reaction of soot in air has been kinetically modeled in several different ways in previous literature but in recent works [8-10] the rate expression in equation 1 has been used most often.

$$-\frac{dm_c}{dt} = A * exp\left[-\frac{E_a}{RT}\right] * [m_c]^{n_c} * \left[P_{O_2}\right]^{n_{O_2}} \quad (1)$$

Using TGA analysis Yang et al. [8] determined that the reaction order for the oxidation reaction of their carbon black model soot, Printex U, was 0.78 and the average activation energy was 138 ± 16 kJ/mol. However, analyzing diesel soot created from a diesel engine running several different operating modes and then deposited on a DPF membrane, two different reaction orders were discovered. During the oxidation of the first ~70% of the soot the reaction order was close to zero, but for the remainder of the oxidation it was 0.8. The activation energies were 154 ± 25 and 153 ± 34 kJ/mol for these two oxidation zones.

Chong et al. [9] performed similar experiments and the reaction order of their surrogate soot was 0.79 with an average activation energy of 148 ± 5 kJ/mol. They also determined the reaction order of oxygen in the reaction to be 0.94. The results from their experiments on soot from a diesel engine showed two separate reaction orders, in agreement with the findings of Yang et al. They did however judge the first zone to cover the first ~80% of the oxidation, with a reaction order of 0.24 ± 0.05 for carbon in zone 1 and 0.74 ± 0.08 in zone 2. The activation energies were 139.55 and 136.26 kJ/mol respectively. The reaction order of oxygen was determined as 0.96 and 0.97 for the two zones, which was not much different from their results with the model soot.

Rodriguez et al. [10] supposed the reaction orders of carbon and oxygen to be unity and compared the reactivity of biodiesel soot with that of regular diesel soot by determining the kinetic parameters of the respective samples. Biodiesel soot was found to have reaction rates 4-14 times higher than regular soot.

3.3.2 Physical structure

Research on the correlations between the morphology of diesel soot and its oxidation reactivity has been done in a variety of ways. One of the more comprehensive studies were performed by Pahalagedara et al. [11], who used several different analysis methods to investigate the relationship between structure and reactivity on two samples of diesel soot from different engines, as well as 10 different commercial carbon black samples. The reactivities were measured using a TGA and then correlated with the structural data. Scanning electron microscopy (SEM) and transmission electron microscopy (TEM) was used to determine the particle sizes, Brunauer−Emmett−Teller (BET) nitrogen sorption revealed the specific surface area and x-ray diffraction (XRD), Raman spectroscopy and TEM was used to investigate the microstructure. These structure-reactivity investigations produced some general trends which showed that highly amorphous soot with low particle size and high surface area possessed a high oxidation reactivity. Conclusions drawn by Yehliu et al. [12] based on XRD and TEM experiments support these correlations between disordered structures and high reactivity. Studies performed by Lapuerta et al. [13], comparing soot produced from biodiesel and regular diesel, using Raman spectroscopy and XRD showed that the more reactive biodiesel soot was less amorphous than soot from regular diesel. This result is contrary to that of Pahalagedara et al., but TEM analysis showed that biodiesel soot had significantly smaller particles and higher surface area, which could account for the higher reactivity despite the less amorphous structure.

3.3.3 Chemical composition

The amount of SOF present in diesel PM varies depending on factors such as fuel composition and engine operating conditions. In previous literature [8-9,14-16] the SOF content in PM normally ranged between 10% and 50% by weight, with levels around 20% being the most common. The impact of SOF on the oxidation reaction of diesel soot in air

has been investigated by TGA. By using different heat treatments in the TGA before oxidation Chong et al. [9] varied the amount of volatile SOF that was evaporated from the soot. The oxidation behavior of the soot was then investigated and it was found that the amount of SOF did not have any significant effect. In a different study Yehliu et al. [14] observed a relationship between the SOF content of the soot and its oxidation reactivity. Soot with a higher volatile SOF content was found to be more reactive but whether the reactivity was directly affected by the SOF content or not was unclear.

The oxidation reactivity is also affected by the amount of surface oxygen groups on the soot but researchers disagree on their influence. Yehliu et al. [12] and Song et al. [17] both studied the oxidation reactivity of biodiesel soot but while Yehliu et al. [12] concluded that the disorder of the soot's carbon structure was more important than the surface oxygen groups, Song et al. [17] asserted that the surface oxygen was more important than the initial structure. Analysis performed by Williams et al. [18] also indicated that the increased oxygen content and disordered structure of biodiesel soot was the main reason for its increased reactivity but did not conclude which factor is the dominant one. Lamharess et al. [19] similarly attributed the higher oxidation rate to increased oxygen content and surface area.

3.3.4 Engine operating conditions

Rodriguez et al. [10] examined the oxidation reactivity for diesel soot derived from three different engine operating modes and two different types of fuel. The engine modes were U9 (low load, low exhaust temperature), EU8 (medium load, exhaust temperature high enough to allow active PDF regeneration) and EU16 (high load, high exhaust temperature which allows for spontaneous regeneration of the PDF). The engine operating conditions were concluded to be of some importance since the temperature required to oxidize the soot varied slightly. Of the tested operating modes EU8 produced the soot which showed the highest temperature requirement. These results are in agreement with those of Lapuerta et al. [13], who performed similar experiments on soot from the same engine operating conditions.

Setiabudi et al. [16] performed a comparison of soot from a diesel engine at idle and full load conditions and found the idle soot to be more reactive to both oxygen and nitrogen dioxide. Interestingly, thermal aging caused the reactivity of the idle soot to drop significantly whereas the full load soot was not affected as much. It should be noted that the idle soot contained a much larger fraction of volatile SOF than the full load soot (about 50% and 20% by weight respectively).

Engine speed and torque was shown to affect the soot reactivity in a study by Yehliu et al. [14]. The results showed that the engine speed had a greater influence than torque on the reactivity and that higher speeds produced a more reactive soot.

Results from experiments done by Al-Qurashi et al. [20] showed that exhaust gas recirculation (EGR) had an influence on the oxidation of diesel soot. Soot produced from an engine running 20% EGR revealed a higher reactivity than 0% EGR soot. It was concluded that the increased reactivity was due to differences in the soot's physical properties, which caused the soot created using EGR to simultaneously burn internally and externally. The soot created without EGR only burned externally.

3.3.5 Fuel

Several researchers [10,13,18-19] have performed studies comparing soot produced from regular diesel with soot from different blends of biodiesel and the results are in agreement that biodiesel soot is oxidized at lower temperatures and with higher reaction rates than normal diesel soot. Lamharess et al. [19] attributed this increased reaction rate to the higher oxygen content and greater surface area of the biodiesel soot.

Uitz et al. [21] investigated the influence of sulfur and aromatic contents in fuel and concluded that the sulfur content had no significant effect on soot oxidation but aromatic content increased the reactivity. The increased reactivity was mainly caused by diaromatics, which through TEM analysis was shown to produce soot with a more distorted morphology.

3.3.6 Oxidation by nitrogen dioxide

Nitrogen dioxide is known to increase the oxidation rate of soot and enable DPF regeneration at lower temperatures. The oxidation involving NO_2 is supposedly initiated by the formation of surface complex intermediates containing oxygen and nitrogen dioxide which are more easily oxidized to CO or CO_2 [16,22]. Through temperature programmed oxidation (TPO) experiments in a flow reactor, Setiabudi et al. [16] compared the reactivity of soot in O_2, NO_2 and a mixture of them both. They concluded that the oxidation reaction by NO_2 is improved by the presence of O_2 and can occur at even lower temperatures than in only NO_2. While examining the kinetics of the oxidation by NO_2 Jacquot et al. [23] noted that the presence of water increased the reaction rate without consuming the water's oxygen and therefore concluded that water catalyzed the reaction.

4 Experiments

4.1 Sample information

A total of 8 different samples of soot created at varying conditions were acquired in order to provide a range of properties which might influence the oxidation reactivity. Samples 1 and 2 were commercially available carbon blacks, Printex U and Vulcan XC 72. Printex U is a commonly used surrogate soot in research on soot oxidation and was therefore deemed a suitable reference material [8,11,16,21,24]. Samples 3-6 consisted of diesel soot from accelerated soot loadings. They were collected from engine cells running on steady state operating conditions with lowered rail pressures. Sample 8 was collected from a similar engine cell where a normal soot loading was being performed without a lowered rail pressure. These diesel soot samples from the engine cells have all passed through a diesel oxidation catalyst before being deposited on the particulate filter. The engine cells were all run on a standard B10 diesel with 10% RME and less than 10 ppm of sulfur. Sample 7 was collected from the EGR inlet manifold of a truck engine and had not passed through a DOC. The truck had been running long haulage for approximately 7000 h and 900 000 km. Table 1 shows a brief summary of the samples.

Table 1. Carbon black and diesel soot samples (* = sample collected from DPF, ¤ = unknown ratio)

Nr	Description & engine	Rail pressure [bar]	EGR [%]	Engine speed [rpm]	Torque [Nm]
1	Printex U				
2	Vulcan XC 72				
3	Accelerated loading, 360hp, 5-cylinder engine*	400	0	1400	300
4	Accelerated loading, 580hp, 8-cylinder engine*	550	40	1800	360
5	Accelerated loading, 360hp, 5-cylinder engine*	400	0	1400	300
6	Accelerated loading, 440hp, 6-cylinder engine*	600	0	1400	650
7	Soot from EGR manifold, 400hp, 6-cylinder engine				
8	Normal loading, 730hp, 8-cylinder engine*	500 - 2500	Yes¤	500 – 1800	-200 – 3000

4.2 Thermogravimetric analysis

In order to determine the oxidation characteristics of the soot samples TGA experiments were performed using a TA Instruments Q500 TGA with an EGA (Evolved Gas Analyzer) Furnace. The samples were placed in a platinum sample pan and devolatilized in a nitrogen gas atmosphere to remove moisture and volatile organic fractions (VOF), followed by oxidation in air according to the process described below:

1. The temperature is increased from room temperature to 500°C with a ramp of 20°C/min in a 10 cm^3/min balance gas flow and 90 cm^3/min sample gas flow, both pure nitrogen gas.
2. The temperature is equilibrated at 500°C and the devolatilization is continued isothermally for 60 min.
3. The sample is then allowed to cool to 50°C and equilibrate.
4. The sample gas is changed from nitrogen to synthetic air with a 20.8% oxygen concentration and the sample is heated to 900°C with a ramp of 10°C/min.

The samples were weighted continuously during this process and the changes in mass and temperature were recorded. The sizes of the samples used in the experiments are presented in Table 2.

Table 2. Sample sizes used in TGA experiments

Sample	Size [mg]
1 - Printex U	6.8
2 - Vulcan XC 72	12.6
3 - 400bar, 0% EGR	1.6
4 - 550bar, 40% EGR	4.4
5 - 400bar, 0% EGR, ash	2.5
6 - 600bar, 0% EGR	1.7
7 - EGR manifold	27.8
8 - Normal loading	0.7

In addition to the experiments described above, samples 3 and 4 were also oxidized without the devolatilization steps in order to compare the oxidation characteristics of devolatilized "dry" soot and as-received "wet" soot, as well as determining if the 60 min thermal aging altered the samples.

Due to a significantly higher VOF content than the other samples, sample 7 was not sufficiently devolatilized after an isothermal period of 60 min. The isothermal step of the devolatilization was therefore increased to 180 min for sample 7 and a new experiment was performed.

4.3 Scanning electron microscopy

The size of the primary particles and the physical structure of the soot samples were investigated using a Zeiss Sigma VP FE-SEM (Field Emission Scanning Electron Microscope). The samples were carefully applied to sample holders with an adhesive carbon tape. The electron beam was operated at 3 kV and images were gathered at 2 000, 20 000 and 200 000 times magnification using the microscope's In-lens detector. Using the images with a magnification of 200 000x, the average diameter of the primary particles were calculated based on measurements on approximately 40 particles from each sample. The carbon/oxygen ratios of the samples were also determined by EDS, using the microscope's Oxford Instruments 50mm^2 X-max SDD (Silicon Drift Detector).

4.4 BET nitrogen sorption

The specific surface area of samples 1, 2 and 7 were determined by a five-point BET (Brunauer, Emmett and Teller) nitrogen sorption analysis, using a Micromeritics ASAP 2000 instrument. This analysis could not be performed on the rest of the samples because the remaining amount of soot was insufficient. Prior to analysis the samples were degassed at 250°C until a pressure of 5 µmHg was reached. The carbon black samples (Printex U and Vulcan XC 72) were sufficiently degassed within 12 h but sample 7 required an excess of 24 h, likely due to the high content of organic compounds. The initial and degassed masses are presented in Table 3.

Table 3. Sample mass prior to BET analysis

Sample	Initial mass [g]	Degassed mass [g]
1 - Printex U	0.26	0.22
2 - Vulcan XC 72	0.27	0.24
7 - EGR manifold	0.24	0.19

4.5 FTIR spectroscopy

The surface functional groups of samples 1-7 were analyzed using a Perkin Elmer Spectrum 100 FTIR with a UATR (Universal Attenuated Total Reflectance) accessory. A diamond/ZnSe crystal was used in the UATR and sets of 32 scans between 650 and 4000cm^{-1} with a resolution of 4 were performed on each sample. The resulting spectra were baseline corrected, normalized and then ATR corrected.

5 Results & discussion

5.1 Thermogravimetric analysis

From the data obtained by the thermogravimetric analyses a general composition of the samples was acquired. The mass loss from evaporation of moisture and volatile organic components was summarized as VOF (Volatile Organic Fraction) and the mass loss due to the oxidation in air was labeled as the soot. The residue left at the end of the oxidation was the ash.

Figure 3 shows the compositions of all samples and it is apparent that for most of them VOF and ash make up only a minor part of the particulate matter. The VOF made up less than 5% of the mass in all samples except for samples 7 and 8, in which it made up 38.8 and 28.4% respectively. These two VOF rich samples are the only ones produced with normal rail pressures and it is possible that the low amount of VOF in the other samples is a result of the accelerated soot loading. It should however be noted that the VOF content of sample 7 could be affected by the fact that it never passed through a DOC. Judging from samples 3 and 5, which were created under identical conditions, the variations in ash content between the samples were likely caused by differences in the sampling process or the DPF's history, e.g. if the DPF had been used in previous soot loadings and regenerations or if it was brand new.

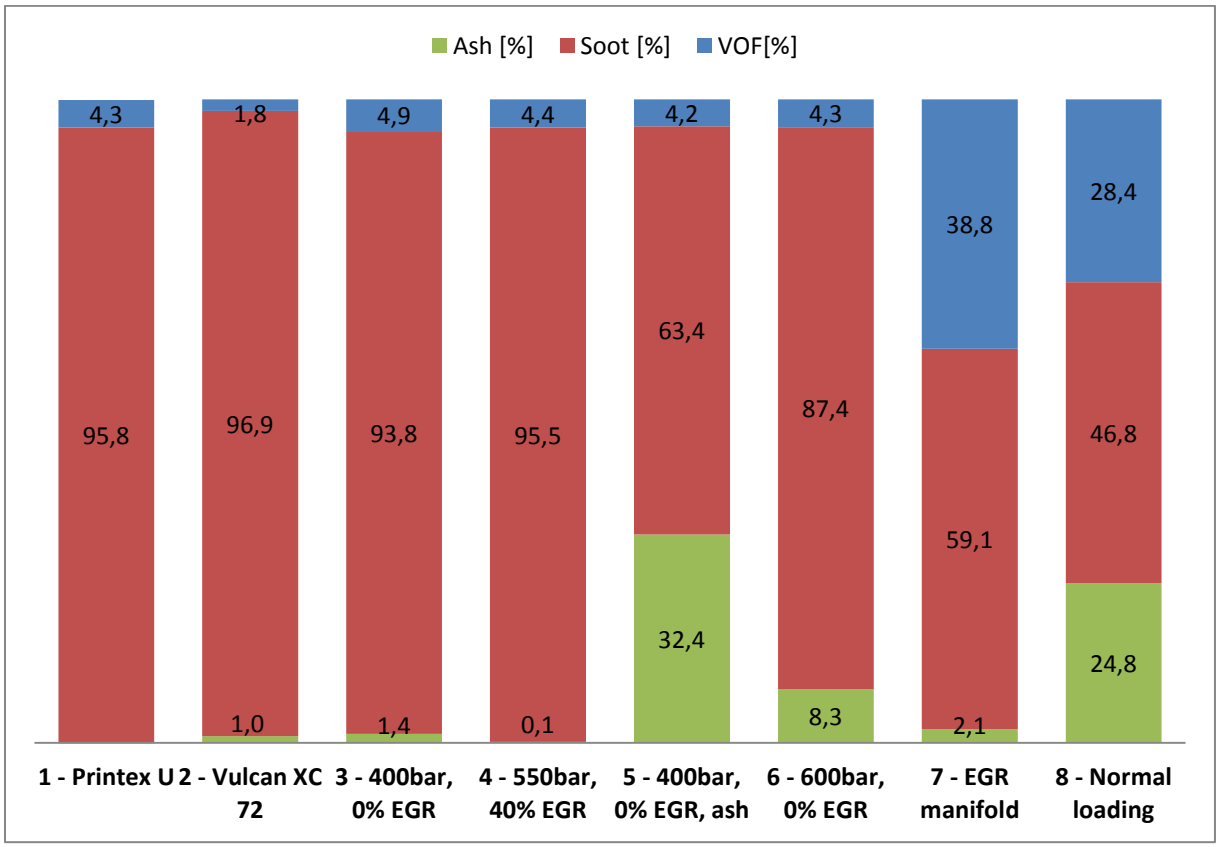

Figure 3. General sample composition based on TGA data

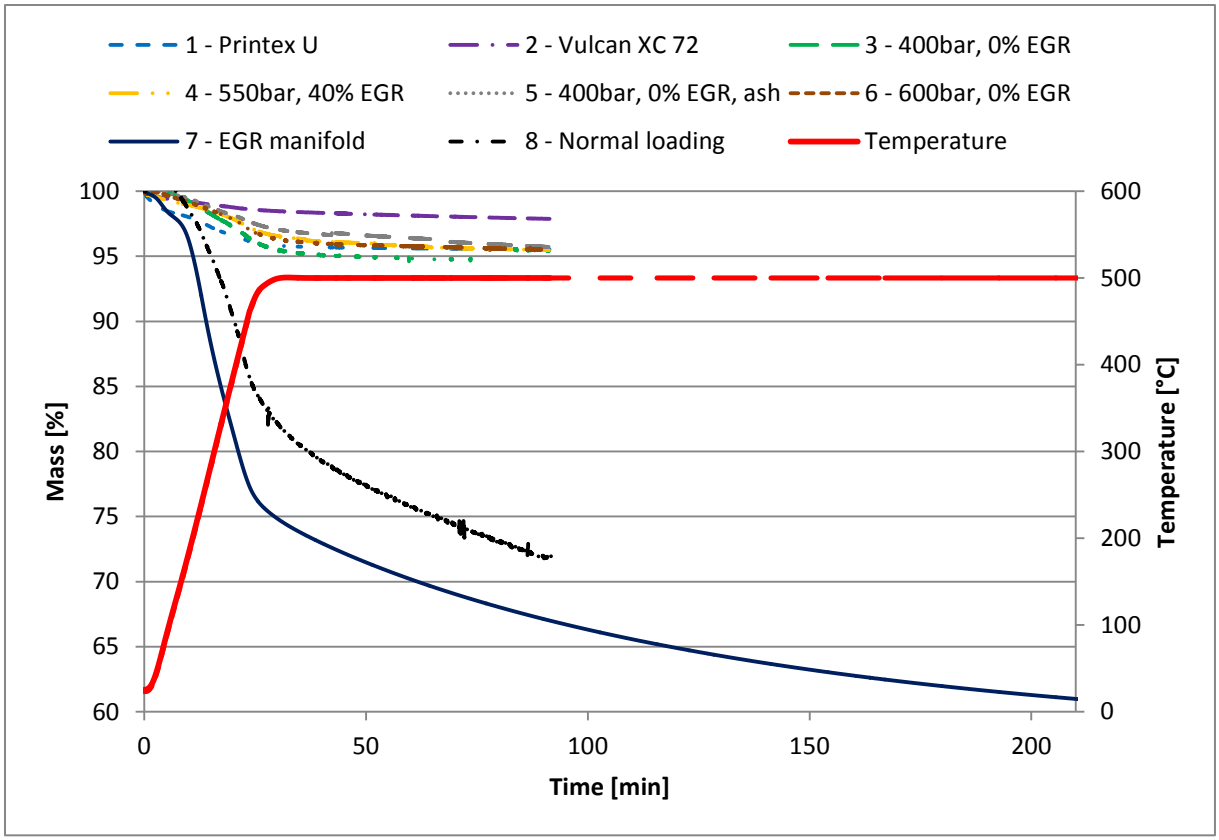

Figure 4. Comparison of the devolatilization step for all samples in the TGA

The drying process of the TGA is shown in Figure 4 and after 60 minutes of the 500°C isothermal the mass loss of samples 1-6 had ceased. The mass loss of sample 7 was clearly not finished after 60 minutes and the isothermal was therefore extended to 180 minutes. Although the mass loss ratio after 180 minutes had decreased significantly, it had not stopped completely. Sample 8 was not fully dried after 60 minutes either, but the lack of sample did not allow for a second analysis with an extended drying step. Consequently it is likely that the actual VOF contents of samples 7 and 8 were slightly higher than the results showed.

The mass losses and mass loss rates are presented graphically in Figure 5 and Figure 6. These graphs show comparisons of how the oxidation progressed for all samples. Samples 1 and 3-6 showed very similar oxidation behaviors, only slightly shifted in temperature in relation to each other. Sample 2 was different in that it had a steeper oxidation curve. It started out slower than the other samples but then there was a sudden drop in mass. The oxidation of sample 7 was also significantly different, taking place at significantly lower temperatures than the other samples and displaying different stages of oxidation. Sample 8 displayed two distinct oxidation stages, the first of which occurring at a relatively low temperature. The second stage was however shifted towards a much higher temperature indicating that a part of the soot in sample 8 was highly unreactive. The unreactive part of the soot was so slow to oxidize that the mass loss had not ceased completely at the end of the TGA experiment, meaning that the ash content of sample 8 likely was slightly less than the result presented in Figure 3.

The difference in oxidation characteristics between devolatilized “dry” soot and as-received “wet” soot were shown to be insignificant for samples 3 and 4, as shown in Figure 7 and Figure 8. The mass loss of the wet samples did start at lower temperatures than with the dry samples due to moisture and VOF being removed but the difference was very small. When the oxidation of the soot took over at temperatures above 500°C there was no longer any discernible difference, which meant that the thermal aging in a nitrogen environment did not significantly alter the samples. Since samples 3 and 4 were both shown to have low levels of VOF (less than 5%) it is possible that soot with significantly higher levels of VOF, such as sample 7, would present greater differences.

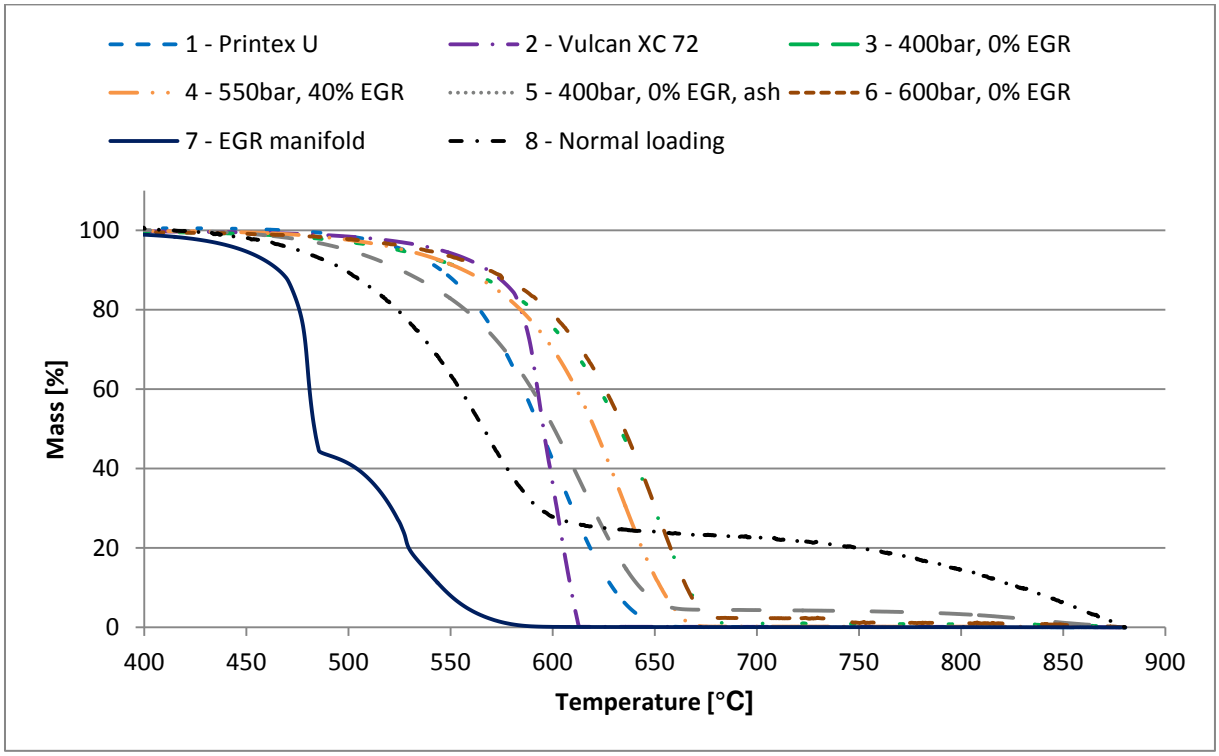

Figure 5. Comparison of the mass loss due to oxidation for all samples in the TGA

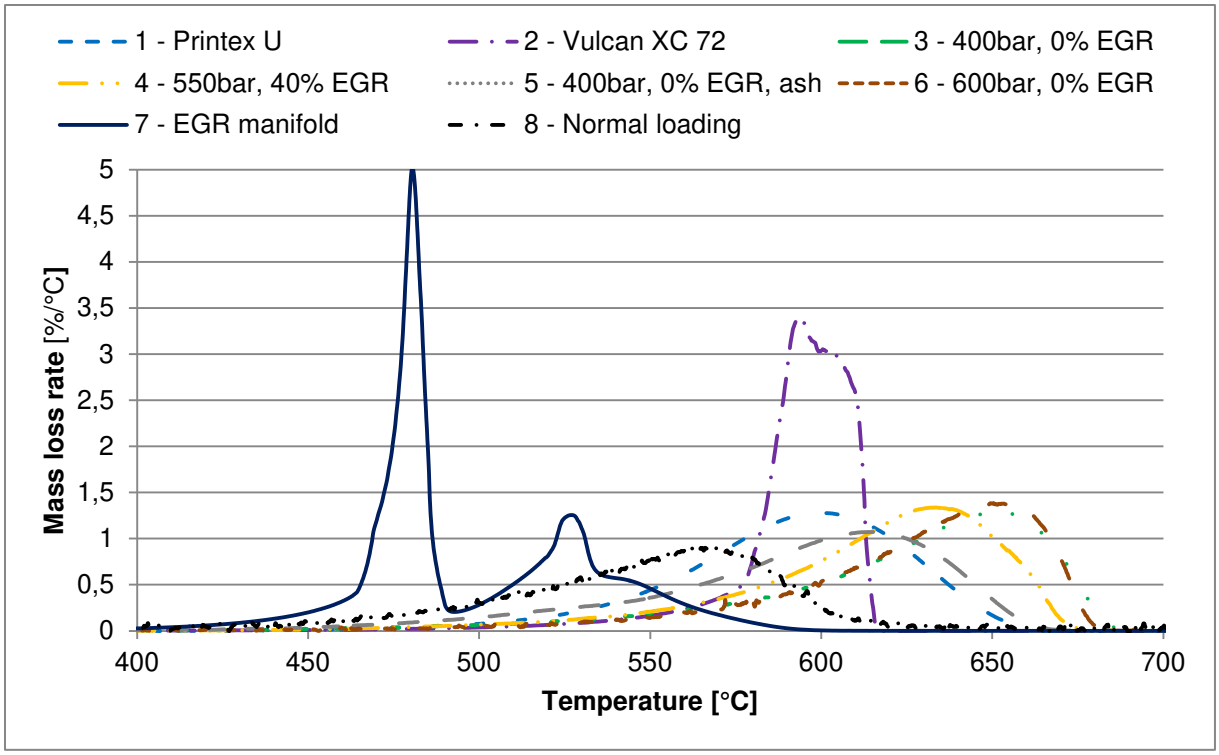

Figure 6. Comparison of the mass loss rate of all samples in the TGA

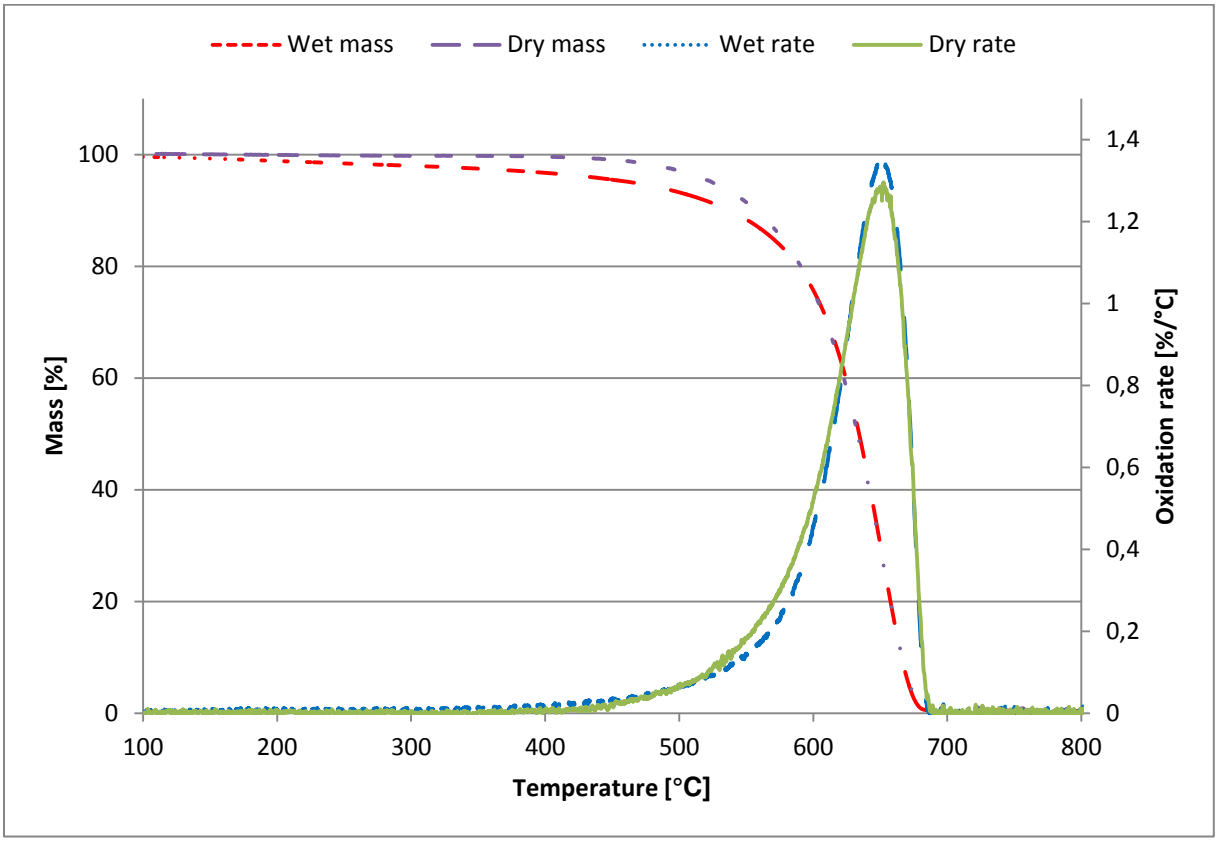

Figure 7. Wet and dry oxidation of sample 3

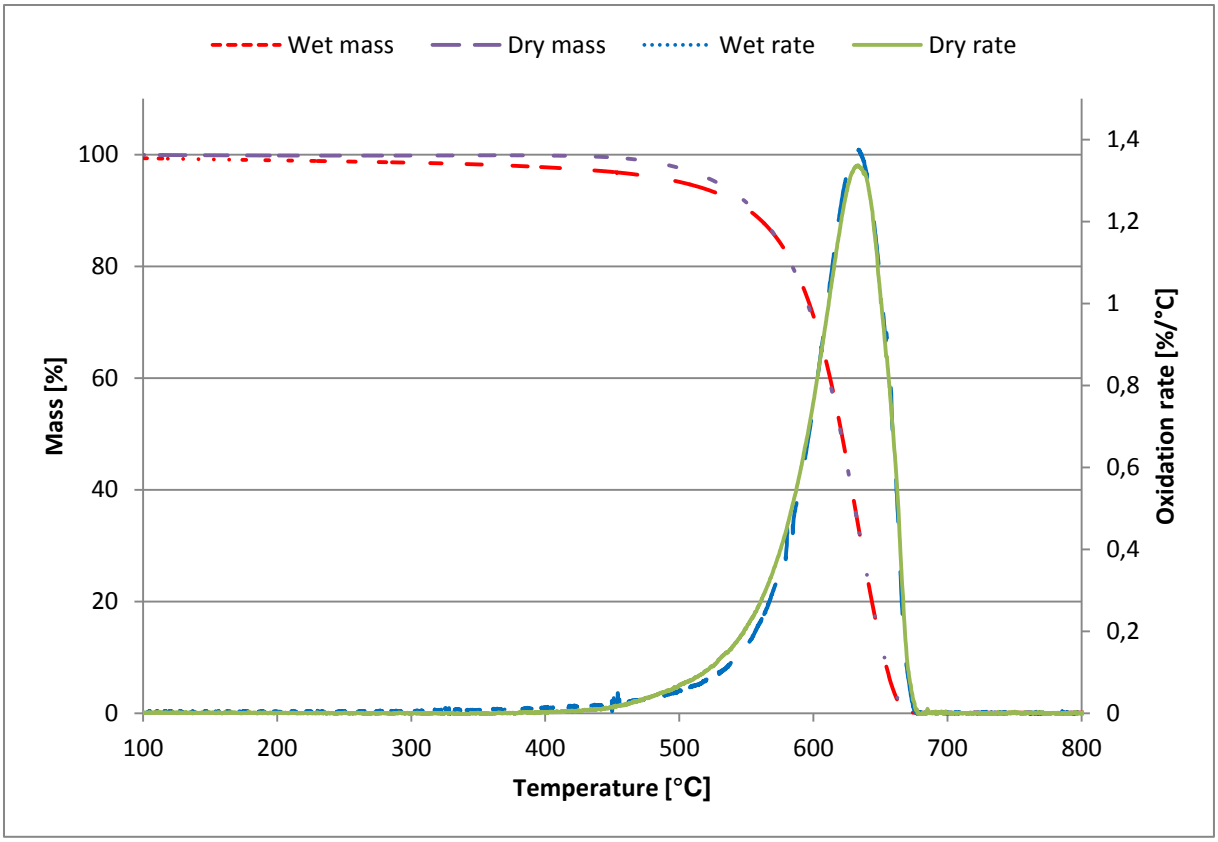

Figure 8. Wet and dry oxidation of sample 4

5.1.1 Oxidation kinetics

The reaction rate expression chosen to model the kinetics of the soot oxidation reactions was the same Arrhenius type equation that was mentioned earlier in the report, equation 1.

$$-\frac{dm_c}{dt} = A * exp\left[-\frac{E_a}{RT}\right] * [m_c]^{n_c} * \left[P_{O_2}\right]^{n_{O_2}} \quad (1)$$

The reaction orders of soot (n_c) and oxygen (n_{O2}) were supposed to be 0.79 and 1 respectively. This was mainly based on previous literature where the reaction order of both model soots as well as the second oxidation zone of diesel soot was found to be 0.79 or close to that value. The reaction order of oxygen was consistently determined to be close to 1 in the same literature. n_c = 0.79 and n_{O2} = 1 was also found to fit relatively well with most of the soot oxidations in this work.

By rearranging equation 1, equation 2 can be obtained. If the logarithms on the left side of the equation are plotted against the inverse of the absolute temperature in a graph it creates an Arrhenius plot. When a straight line is adapted to the graph the y-axis intercept and slope of that line can be used to calculate the activation energy (E_a) and pre-exponential factor (A).

$$\ln\left[-\frac{dm_c}{dt}\right] - n_c * \ln[m_c] = \ln\left[A * P_{O_2}\right] - \left[\frac{E_a}{R}\right] * \left[\frac{1}{T}\right] \quad (2)$$

Arrhenius plots for samples 1-8 are presented in figures 9-18. Only the oxidation of the soot content in the samples was plotted and used to determine the kinetic parameters.

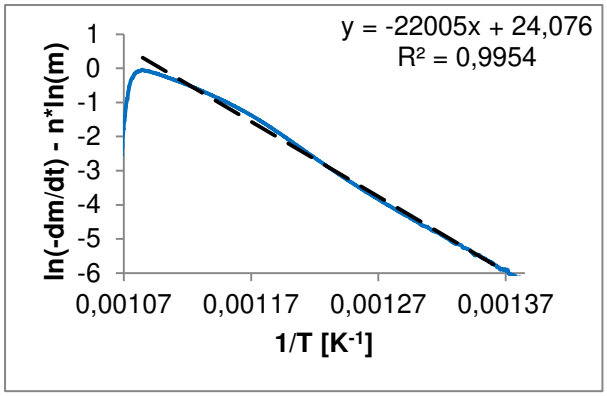

Figure 9. Arrhenius plot of 1 - Printex U. Linear interval from 467 to 653°C, encompassing 99.5% of the soot oxidation

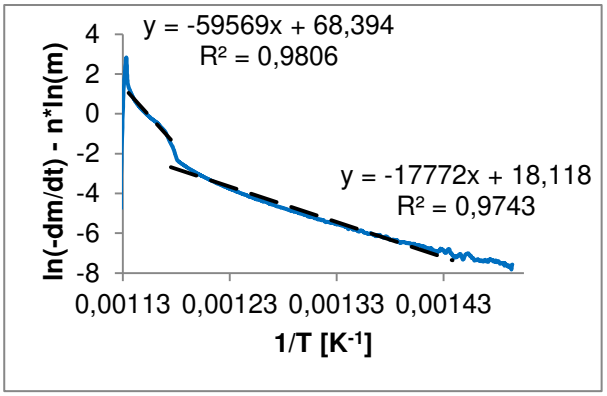

Figure 10. Arrhenius plot of 2 - Vulcan XC 72. Linear intervals from 424 to 582°C and 582 to 611°C, encompassing 16.0 and 80.2% of the soot oxidation respectively

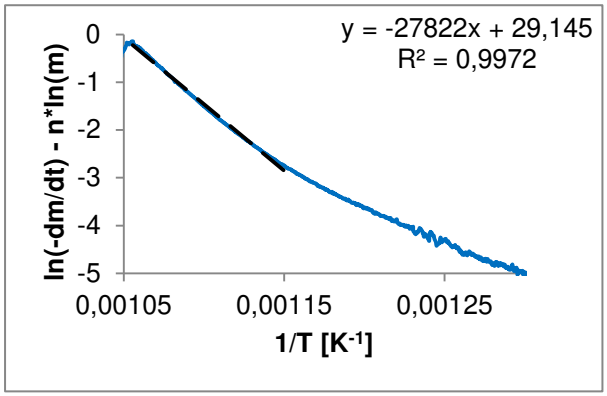

Figure 11. Arrhenius plot of 3 - 400bar, 0% EGR. Linear interval from 596 to 674°C, encompassing 73.8% of the soot oxidation

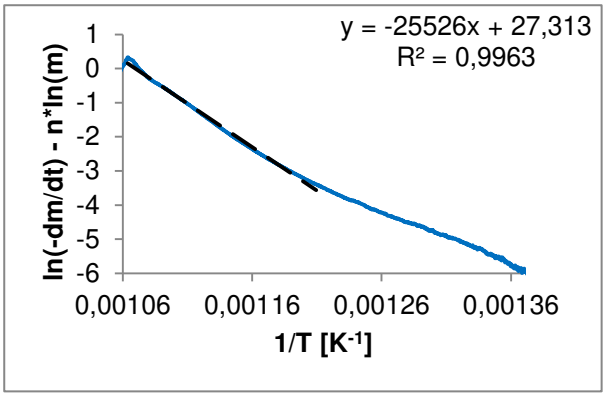

Figure 12. Arrhenius plot of 4 - 550bar, 40% EGR. Linear interval from 554 to 667°C, encompassing 89.6% of the soot oxidation

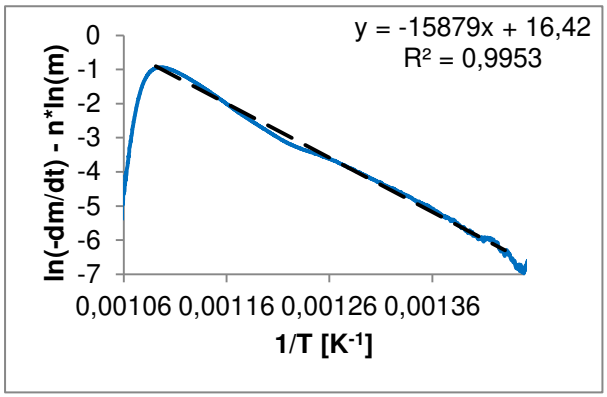

Figure 13. Arrhenius plot of 5 - 400bar, 0% EGR, ash. Linear interval from 426 to 643°C, encompassing 90.0% of the soot oxidation

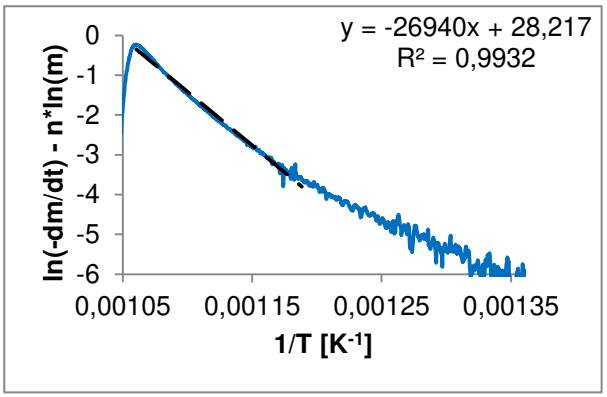

Figure 14. Arrhenius plot of 6 - 600bar, 0% EGR. Linear interval from 568 to 670°C, encompassing 84.1% of the soot oxidation

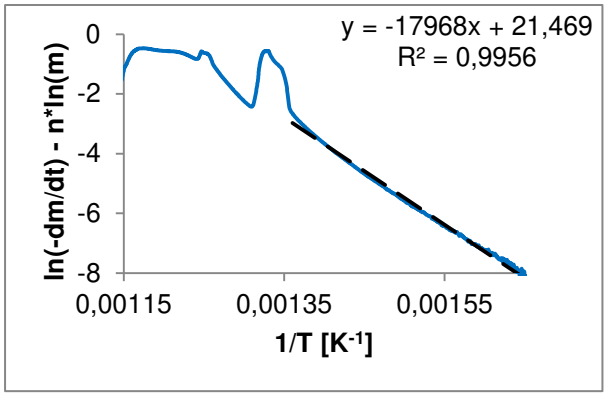

Figure 15. Arrhenius plot of 7 - EGR manifold. Linear interval from 333 to 462°C, encompassing 8.0% of the soot oxidation

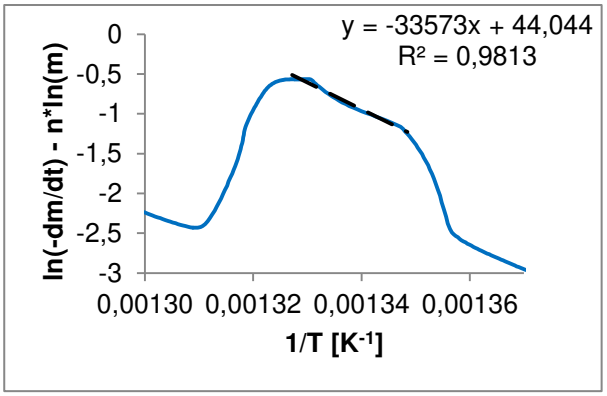

Figure 16. Arrhenius plot of 7 - EGR manifold Linear interval from 468 to 480°C, encompassing 25.4% of the soot oxidation

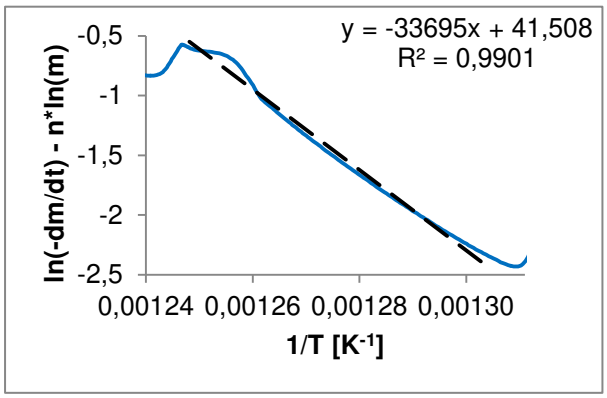

Figure 17. Arrhenius plot of 7 - EGR manifold. Linear interval from 493 to 528°C, encompassing 20.5% of the soot oxidation

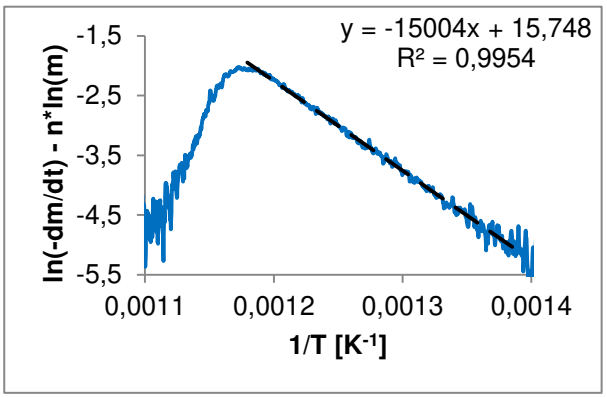

Figure 18. Arrhenius plot of 8 - Normal loading. Linear interval from 446 to 575°C, encompassing 55.9% of the soot oxidation

The linear intervals in the Arrhenius plots represent the oxidation zones of the soot samples and as figures 9-18 show, most of these samples presented a single oxidation zone which covered almost the entire oxidation process. One of the exceptions was sample 2 in Figure 10, which had two separate oxidation zones. The first zone had a much wider temperature span than the second zone but only a minor part of the oxidation occurred in it. The second zone was where over 80% of the oxidation took place. The other exception was sample 7, which had several different oxidation zones. Similarly to sample 2, the first zone (shown in Figure 15) had a wide temperature span but only minor oxidation. The two narrow zones in Figure 16 and Figure 17 were more important since they together covered almost half of the total oxidation. Their linear equations were also extremely similar, which meant that the derived activation energy and pre-exponential factor were almost identical.

The activation energies and pre-exponential factors from each sample's most relevant oxidation zone are presented in Table 4. The activation energies provide a means of comparing the temperatures at which the oxidations occur, with lower activation energies indicating lower oxidation temperatures and vice versa. Additionally, high pre-exponential factors are indicators of high oxidation rates. The activation energy of Printex U was found to be slightly higher than the results of Yang et al. [8]. A possible explanation for the difference is the TGA method. Yang et al. [8] used a set of three isothermal oxidations whereas the experiments in this work used a temperature ramp.

Table 4. Activation energies and pre-exponential factors of soot samples

Sample	Ea [kJ/mol]	A [Pa^{-1} s^{-1}]
1 - Printex U	183	$2.5*10^{4}$
2 - Vulcan XC 72	495	$4.4*10^{23}$
3 - 400bar, 0% EGR	231	$4.0*10^{6}$
4 - 550bar, 40% EGR	212	$6.4*10^{5}$
5 - 400bar, 0% EGR, ash	132	11.9
6 - 600bar, 0% EGR	224	$1.6*10^{6}$
7 - EGR manifold	279	$7.2*10^{19}$
8 - Normal loading	125	6.1

5.1.2 Characteristic temperatures

Using certain characteristic temperatures from the oxidation process is not only a way of comparing the reactivity of different samples but also a relatively easy means of correlating different soot properties to the reactivity. The five characteristic temperatures used for comparison of the samples are: SOT (Starting Oxidation Temperature), $MLRT_{max}$ (Maximum Mass Loss Rate Temperature), FOT (Final Oxidation Temperature), T10 and T50 (temperatures when 10% and 50% of the soot have been oxidized). Figure 19 demonstrates which points in the oxidation these temperatures represent.

In Figure 20 these five characteristic temperatures from all samples are compared against each other, with the exception of sample 8 lacking a FOT temperature since the oxidation had not been completed at the end of the experiment. The two non-accelerated samples (7 & 8) were shown to have the lowest oxidation temperatures at all five points, except for the FOT of sample 8.

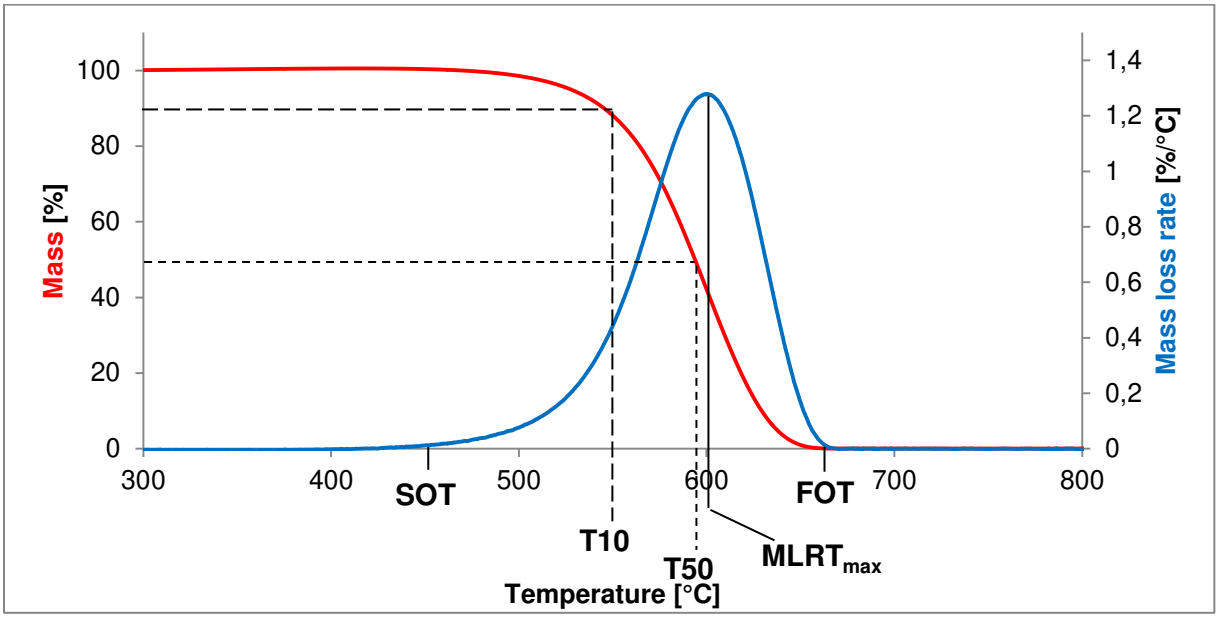

Figure 19. Mass and mass loss rate for 1 - Printex U

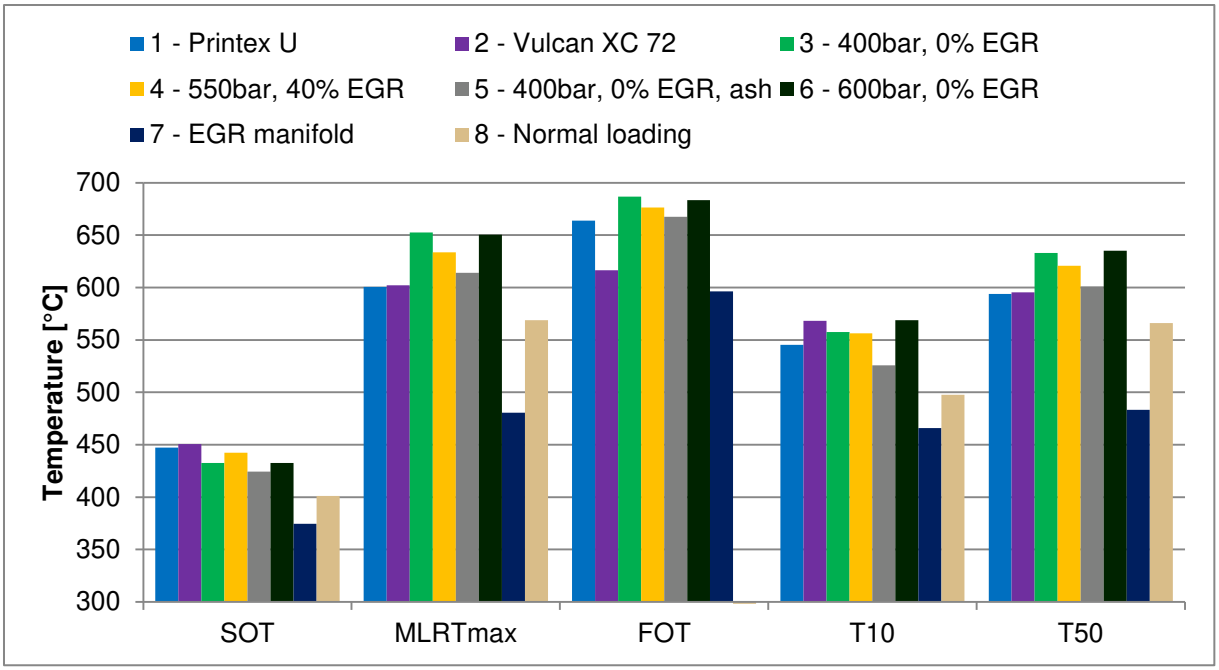

Figure 20. Sample comparison at different characteristic temperatures

There is a small concern that the irregular sample sizes may have affected the results slightly. Rodriguez et al. [10] showed that the characteristic temperatures of the oxidation were dependent on the initial sample mass, particularly for samples below 3 mg. The repeatability of the characteristic temperatures was also negatively affected by such small samples.

5.2 Scanning electron microscopy

The images of the soot samples gathered at 20 000x magnification displayed varying degrees of porosity. Sample 8 (visible in Figure 21) was one of the samples which appeared most porous, with samples 4 and 6 showing similar porous structures. Sample 7 (Figure 22) displayed the most dense looking structure and the remaining samples were somewhere in-between.

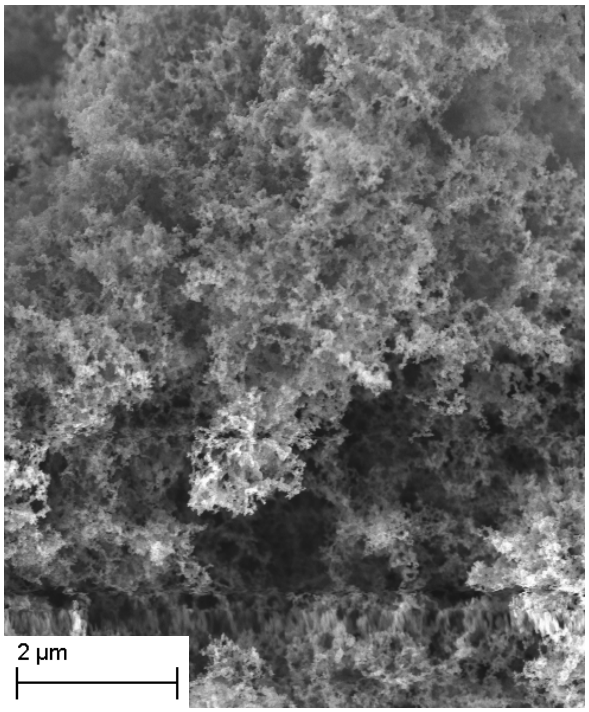

Figure 21. Sample 8 - Normal loading, 20 000x magnification

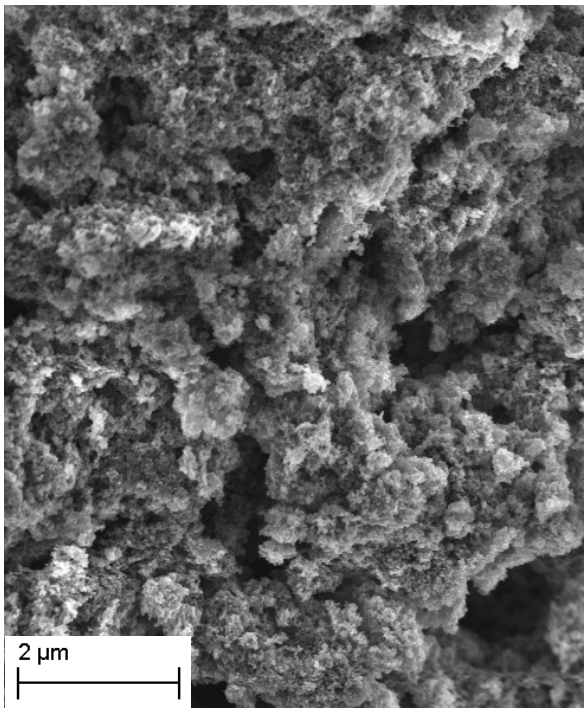

Figure 22. Sample 7 - EGR manifold, 20 000x magnification

The average diameter of the soot's primary particles, presented in Figure 23, were calculated from measurements on the images with a magnification of 200 000x. These images can be seen in Appendix I – SEM images, 200 000x magnification. All samples had a very similar particle size with an average diameter around 40 nm, except for sample 8 which had slightly smaller primary particles with an average size just below 30nm. In previous literature the primary particles of diesel soot had average sizes in the range of 20 – 70nm [11,13,20,25]. Neither the porosity nor the particle size could be clearly correlated to a change in reactivity since the two most reactive samples (7 and 8) were at opposite ends in terms of porosity and the difference in particle size between most samples was negligible.

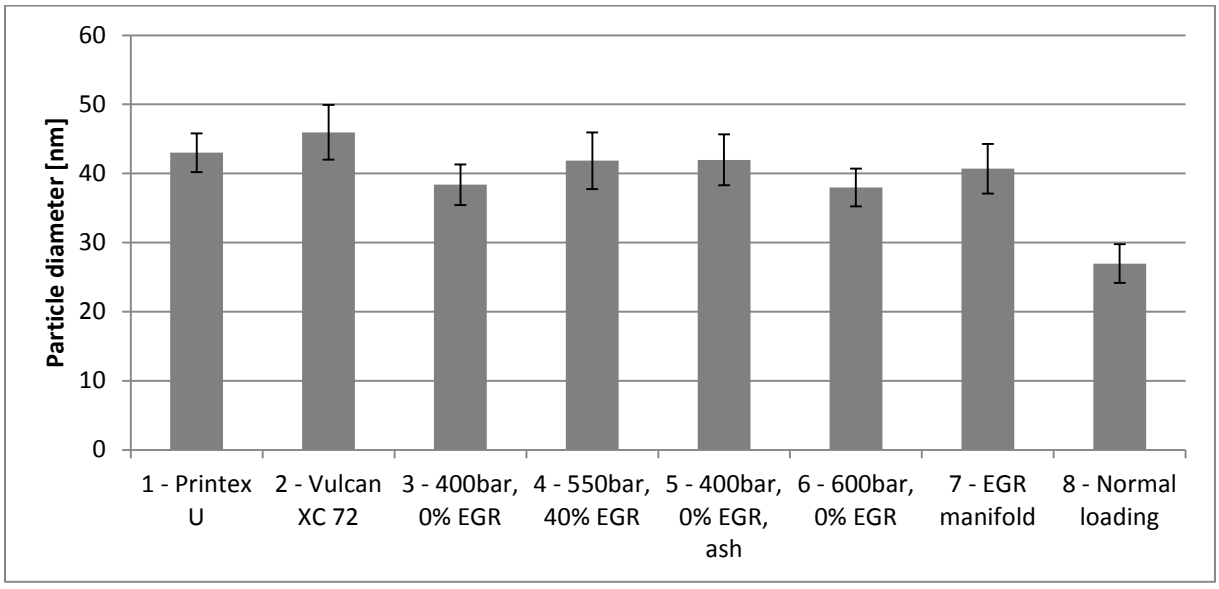

Figure 23. Average diameter of the primary particles

5.2.1 Energy dispersive x-ray spectroscopy

The EDS analysis was not accurate enough to provide the exact oxygen content of the soot but the amount of oxygen relative to the amount of carbon in the soot was determined. Table 5 displays the relative amounts of oxygen and carbon in each sample as well as a calculated oxygen/carbon ratio. Most samples had similarly low O/C ratios but samples 5, 7 and 8 stood out with significantly higher ratios. Since these were the samples with high ash or VOF contents, the increased O/C ratios were likely caused by oxygen in the VOF's organic compounds or the ash's metal oxides. The high O/C ratios also coincide with more reactive soot. These results should only be viewed as a hint of the oxygen content in the soot and other elemental analyses are required to accurately determine the actual content.

Table 5. Oxygen/carbon ratio from EDS analysis

Sample	C [%]	O [%]	O/C ratio
1 - Printex U	98	2	0.02
2 - Vulcan XC 72	99	1	0.01
3 - 400bar, 0% EGR	96	4	0.04
4 - 550bar, 40% EGR	96	4	0.04
5 - 400bar, 0% EGR, ash	89	11	0.1
6 - 600bar, 0% EGR	97	3	0.03
7 - EGR manifold	90	10	0.1
8 - Normal loading	91	9	0.1

5.3 BET nitrogen sorption

The results from the surface area analysis can be viewed in Table 6. It is apparent that there were significant variations in the specific surface area but the samples were too few to discern any correlations between oxidation reactivity and surface area. The result for Printex U is fairly similar to that of Pahalagedara et al. [11], who determined the specific surface area to be 96 m^2/g.

Table 6. Specific surface area results from BET analysis

Sample	Specific surface area [m^2/g]
1 - Printex U	111
2 - Vulcan XC 72	265
7 - EGR manifold	149

5.4 FTIR spectroscopy

In Figure 24 the transmission spectra of samples 1-7 have been overlaid and a few peaks of interest have been labeled. In the spectrum from sample 7 the two peaks at 2910 cm^{-1} and 2840 cm^{-1} were significantly more pronounced than in the other spectra. These peaks were positioned within the assignment regions for the C-H stretching in alkanes. This result matches the established high VOF content of sample 7. The spectrum from sample 5 had a peak which stood out from the other spectra at 1090 cm^{-1}. A peak in that assignment region most likely indicates phosphine or sulphate groups, which in sample 5 coincides with a high ash content.

FTIR spectroscopy was not well suited for analysis of soot because there was a high absorption across the entire spectrum with very broad peaks that very often overlapped and obscured each other. Only samples with significantly different compositions showed any distinct differences in the spectra.

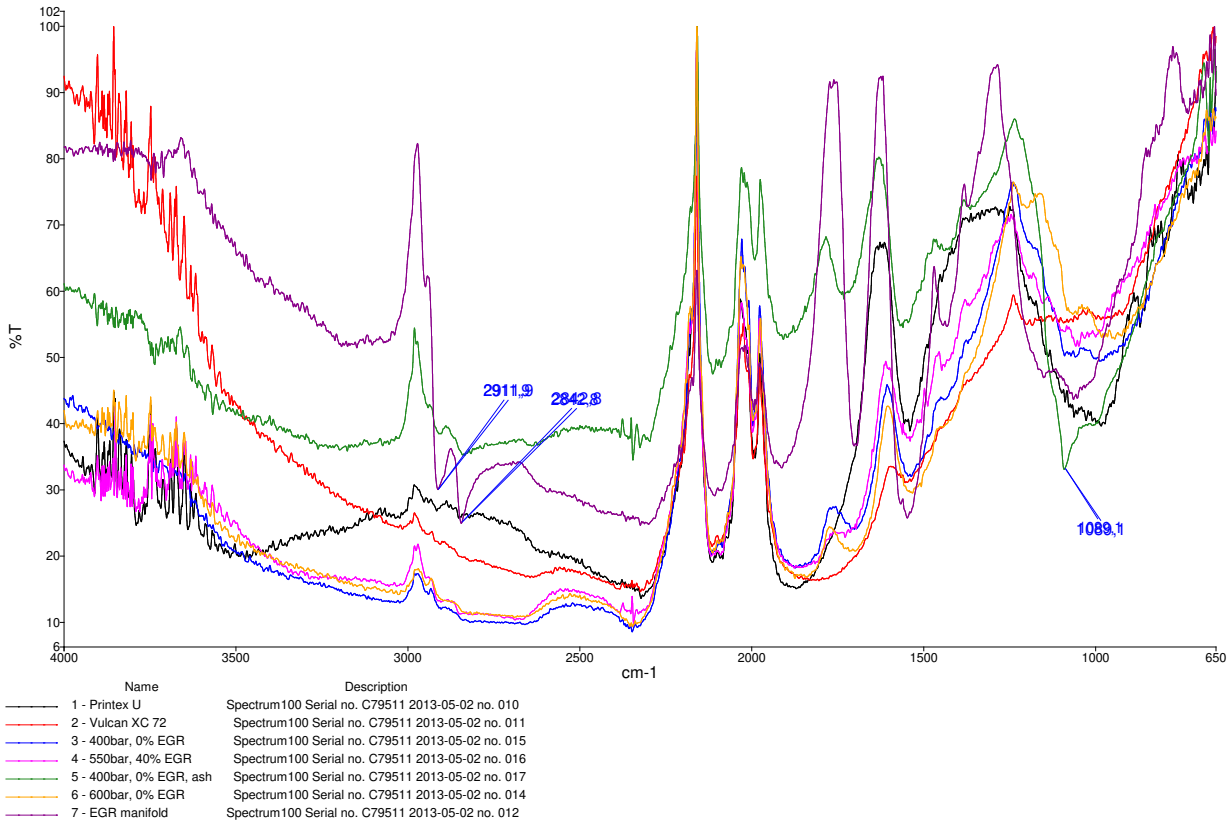

Figure 24. Baseline corrected, normalized and ATR corrected FTIR transmission spectra of samples 1-7

6 Conclusions

Based on the results from this work it has been concluded that soot created during accelerated soot loading with decreased rail pressure was different from soot created with normal rail pressure. The accelerated soot had a lower VOF content and was oxidized at slightly higher temperatures than normal soot. There was also a difference in oxidation behavior, with the accelerated soot displaying only a single oxidation zone whereas normal soot was oxidized in several steps.

The type of soot that displayed the highest reactivity was soot that had a high oxygen content (oxygen/carbon ratio) and a high VOF content.

The thermogravimetric analysis was the most important of all methods used in this work. Not only did it provide the rudimentary compositions of the samples and the means to compare the reactivity of the soot in several different ways, it also provided the data required to formulate rate expressions for the oxidation reactions.

Using a very small amount of sample, the scanning electron microscope captured images which showed the structure of the larger soot particles as well as the size of the smaller primary particles. No clear correlations between these factors and the reactivity were found however. The oxygen/carbon ratio provided by the energy dispersive x-ray spectroscopy allowed for a simple means of comparing the general oxygen content of the samples. All things considered, the SEM-EDS was a worthwhile addition to the analysis methods.

The BET surface area analysis required a large sample size compared to the other methods, which ruled it out for use on the smaller samples. This meant that no conclusions were drawn regarding the effect of the soot's specific surface area.

The FTIR analysis proved to be the least useful technique for soot analysis. The soot had a high absorption across the entire spectrum and much overlapping of the peaks, which made the results problematic to interpret.

7 Recommendations for further work

- Thermogravimetric analyses of soot with a gas similar to diesel exhaust gases should provide more accurate information on the oxidation characteristics of diesel soot during DPF regeneration. The presence of NO_2 is of particular interest since it has a profound effect on the oxidation of soot.
- Comparisons of accelerated and normal soot samples produced under otherwise identical conditions (same engine, fuel, speed etc.) should provide more definitive results on how much accelerated soot differs from normal soot.
- By running isothermal TGAs the reaction order of the soot can be experimentally determined. This would allow for more accurate oxidation rate expressions to be formulated.
- Possible correlations between the soot's specific surface area and oxidation reactivity should be investigated further since previous studies indicate that it affects the reactivity.
- Investigate the influence of different diesel fuels since much of the literature suggest that the fuel composition has a significant effect on the reactivity of the soot that is created.

It should be noted that as much information as possible about the soot's history is required in order to be able to compare the reactivity of different samples. It is important to know not only the fuel composition and engine operating conditions, but also how the soot has thermally aged in contact with the exhaust gases and how the sampling of the soot is performed, since these factors also affect the soot.

8 References

[1] "Emission Standards: Heavy-Duty Truck and Bus Engines," DieselNet, 2012. [Online]. Available: http://www.dieselnet.com/standards/eu/hd.php. [Accessed 15 April 2013].

[2] W. A. Majewski, "Diesel Particulate Matter," DieselNet, 2002. [Online]. Available: http://www.dieselnet.com/tech/dpm.php. [Accessed 3 April 2013].

[3] M. K. Khair and H. Jääskeläinen, "Combustion in Diesel Engines," DieselNet, 2010. [Online]. Available: http://www.dieselnet.com/tech/diesel_comb.php. [Accessed 3 April 2013].

[4] M. K. Khair and H. Jääskeläinen, "Emission Formation in Diesel Engines," DieselNet, 2008. [Online]. Available: http://www.dieselnet.com/tech/diesel_emiform.php. [Accessed 3 April 2013].

[5] M. Votsmeier, T. Kreuzer, J. Gieshoff and G. Lepperhoff, "Automobile Exhaust Control," in *Ullmann's Encyclopedia of Industrial Chemistry*, Wiley-VCH Verlag GmbH & Co. KGaA, 2000.

[6] W. A. Majewski, "Diesel Particulate Filters," DieselNet, 2011. [Online]. Available: http://www.dieselnet.com/tech/dpf.php. [Accessed 4 April 2013].

[7] W. A. Majewski, "Diesel Filter Regeneration," DieselNet, 2005. [Online]. Available: http://www.dieselnet.com/tech/dpf_regen.php. [Accessed 4 April 2013].

[8] S. Yang, K. Lee and H. Chong, "Characterization of Oxidation Behaviors and Chemical-Kinetics Parameters of Diesel Particulates Relevant to DPF Regeneration," SAE Technical Paper 2010-01-2166, 2010, doi:10.4271/2010-01-2166.

[9] H. S. Chong, S. K. Aggarwal, K. O. Lee, S. Y. Yang and H. Seong, "Experimental Investigation on the Oxidation Characteristics of Diesel Particulates Relevant to DPF Regeneration," *Combustion Science and Technology,* vol. 185, no. 1, pp. 95-121, 2012.

[10] J. Rodríguez-Fernández, F. Oliva and R. A. Vázquez, "Characterization of the Diesel Soot Oxidation Process through an Optimized Thermogravimetric Method," *Energy & Fuels,* vol. 25, no. 5, pp. 2039-2048, 2011.

[11] L. Pahalagedara, H. Sharma, C.-H. Kuo, S. Dharmarathna, A. Joshi, S. L. Suib and A. B. Mhadeshwar, "Structure and Oxidation Activity Correlations for Carbon Blacks and Diesel Soot," *Energy & Fuels,* vol. 26, no. 11, pp. 6757-6764, 2012.

[12] K. Yehliu, R. L. Vander Wal, O. Armas and A. L. Boehman, "Impact of fuel formulation on the nanostructure and reactivity of diesel soot," *Combustion and Flame,* vol. 159, no. 12, pp. 3597-3606, 2012.

[13] M. Lapuerta, F. Oliva, J. R. Agudelo and A. L. Boehman, "Effect of fuel on the soot nanostructure and consequences on loading and regeneration of diesel particulate

filters," *Combustion and Flame,* vol. 159, no. 2, pp. 844-853, 2012.

[14] K. Yehliu, O. Armas, R. L. Vander Wal and A. L. Boehman, "Impact of engine operating modes and combustion phasing on the reactivity of diesel soot," *Combustion and Flame,* vol. 160, no. 3, pp. 682-691, 2013.

[15] H. Chong, S. Y. Yang and K. O. Lee, "Accurate Measurements of Heat Release, Oxidation Rates, and Soluble Organic Compounds of Diesel Particulates through Thermal Reactions," SAE Technical Paper 2010-01-0814, 2010, doi:10.4271/2010-01-0814.

[16] A. Setiabudi, M. Makkee and J. A. Moulijn, "The role of NO_2 and O_2 in the accelerated combustion of soot in diesel exhaust gases," *Applied Catalysis B: Environmental,* vol. 50, no. 3, pp. 185-194, 2004.

[17] J. Song, M. Alam, A. L. Boehman and U. Kim, "Examination of the oxidation behavior of biodiesel soot," *Combustion and Flame,* vol. 146, no. 4, pp. 589-604, 2006.

[18] A. Williams, R. L. McCormick, R. R. Hayes, J. Ireland and H. L. Fang, "Effect of Biodiesel Blends on Diesel Particulate Filter Performance," 2006.

[19] N. Lamharess, C.-N. Millet, L. Starck, E. Jeudy, J. Lavy and P. Da Costa, "Catalysed diesel particulate filter: Study of the reactivity of soot arising from biodiesel combustion," *Catalysis Today,* vol. 176, no. 1, pp. 219-224, 2011.

[20] K. Al-Qurashi and A. L. Boehman, "Impact of exhaust gas recirculation (EGR) on the oxidative reactivity of diesel engine soot," *Combustion and Flame,* vol. 155, no. 4, pp. 675-695, 2008.

[21] R. Uitz, R. Cracknell, H. Jansma and M. Makkee, "Impact of Diesel Fuel Composition on Soot Oxidation Characteristics," SAE Technical Paper 2009-01-0286, 2009, doi:10.4271/2009-01-0286.

[22] P. Ehrburger, J. F. Brilhac, Y. Drouillot, V. Logie and P. Gilot, "Reactivity of Soot With Nitrogen Oxides in Exhaust Stream," SAE Technical Paper 2002-01-1683, 2002, doi:10.4271/2002-01-1683.

[23] F. Jacquot, V. Logie, J. F. Brilhac and P. Gilot, "Kinetics of the oxidation of carbon black by NO_2: Influence of the presence of water and oxygen," *Carbon,* vol. 40, no. 3, pp. 335-343, 2002.

[24] J. P. Neeft, T. X. Nijhuis, E. Smakman, M. Makkee and J. A. Moulijn, "Kinetics of the oxidation of diesel soot," *Fuel,* vol. 76, no. 12, pp. 1129-1136, 1997.

[25] M. Ahmadinejad, A. Tsolakis, J. M. Becker, C. F. Goersmann, A. D. Newman and T. C. Watling, "Modelling of Soot Oxidation by NO_2 in a Diesel Particulate Filter," *SAE Int. J. Fuels Lubr.,* vol. 5, no. 1, pp. 359-369, 2011.

Appendix I – SEM images, 200 000x magnification

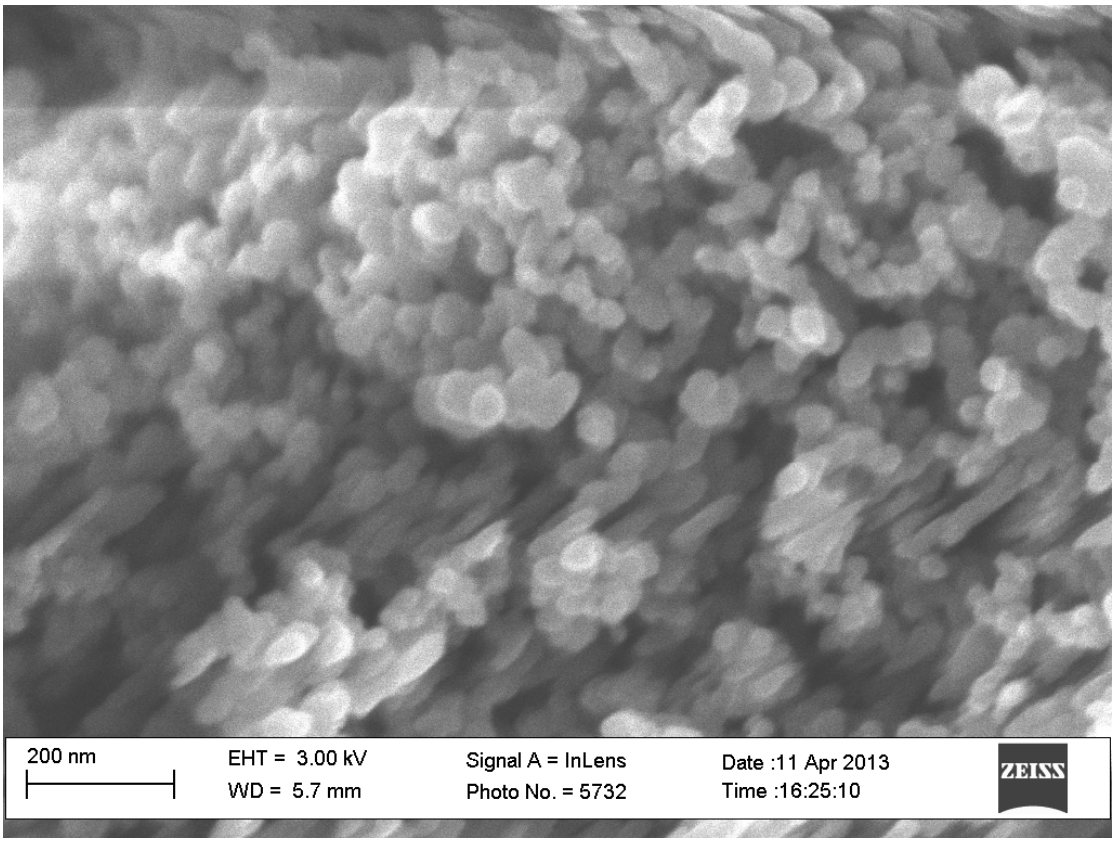

Figure 25. 1 - Printex U

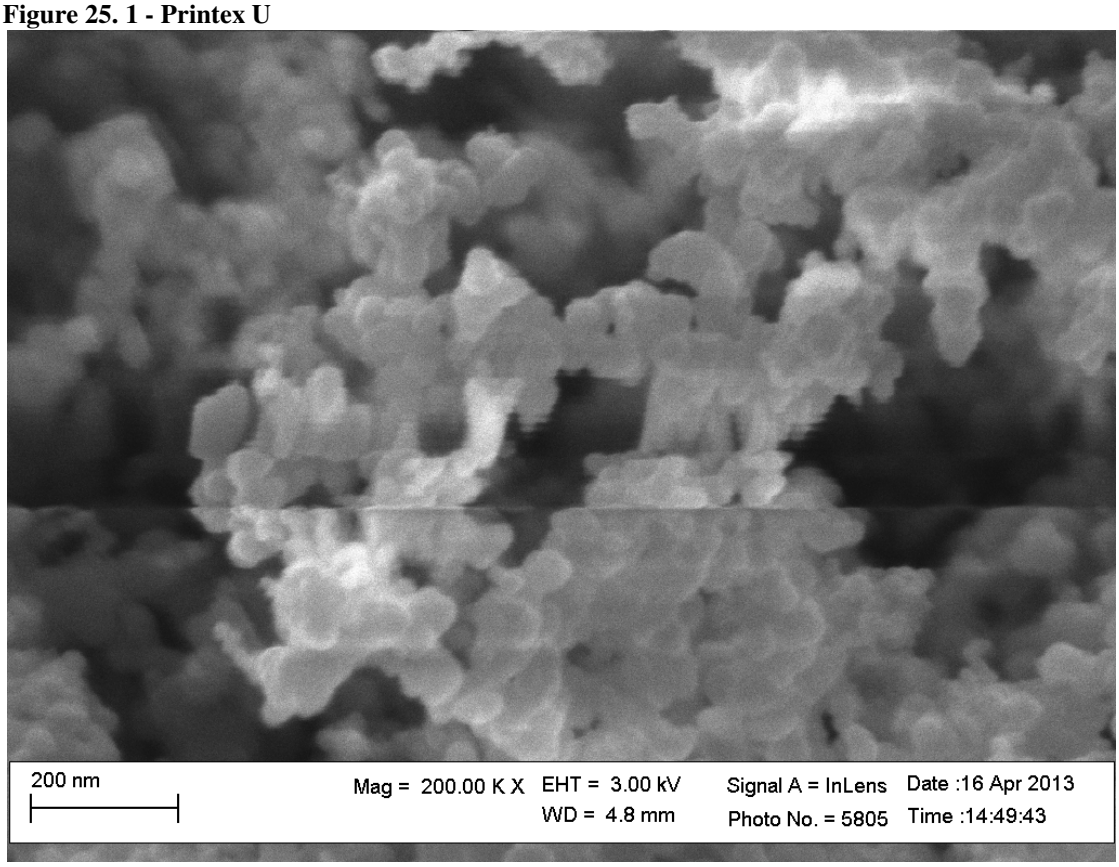

Figure 26. 2 - Vulcan XC 72

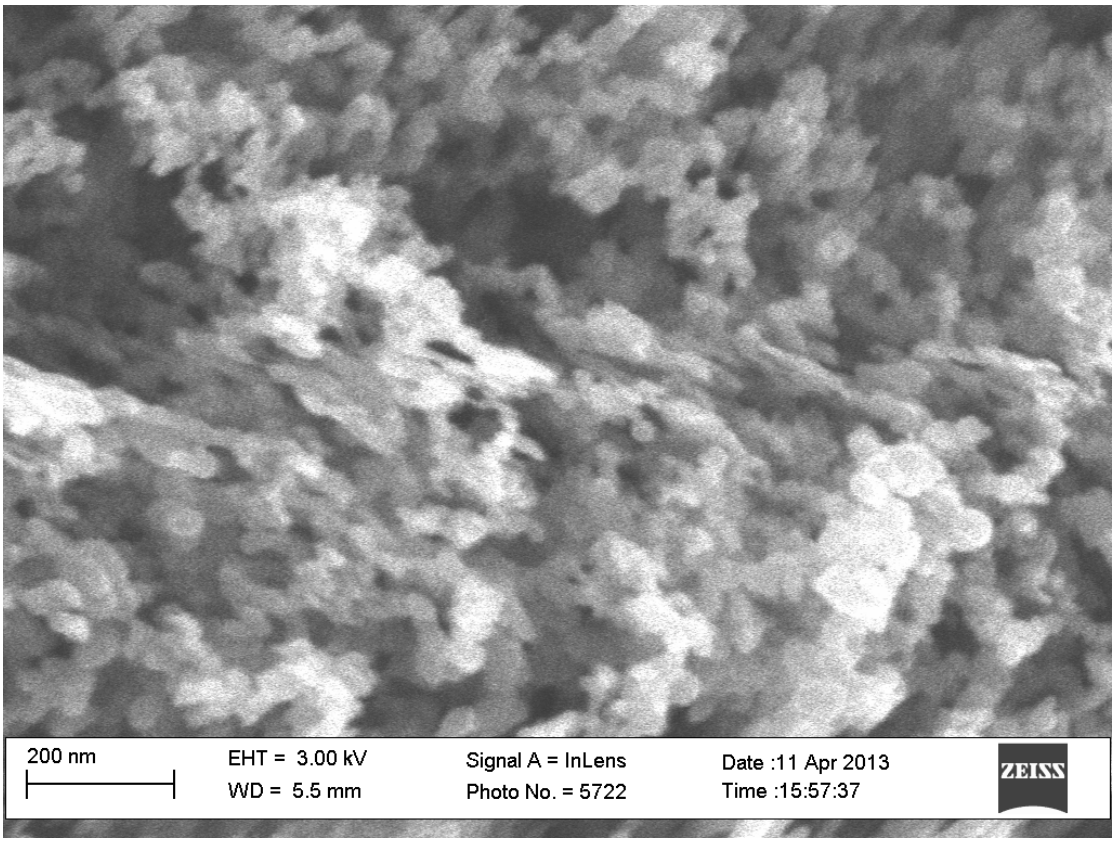

Figure 27. 3 - 400bar, 0% EGR

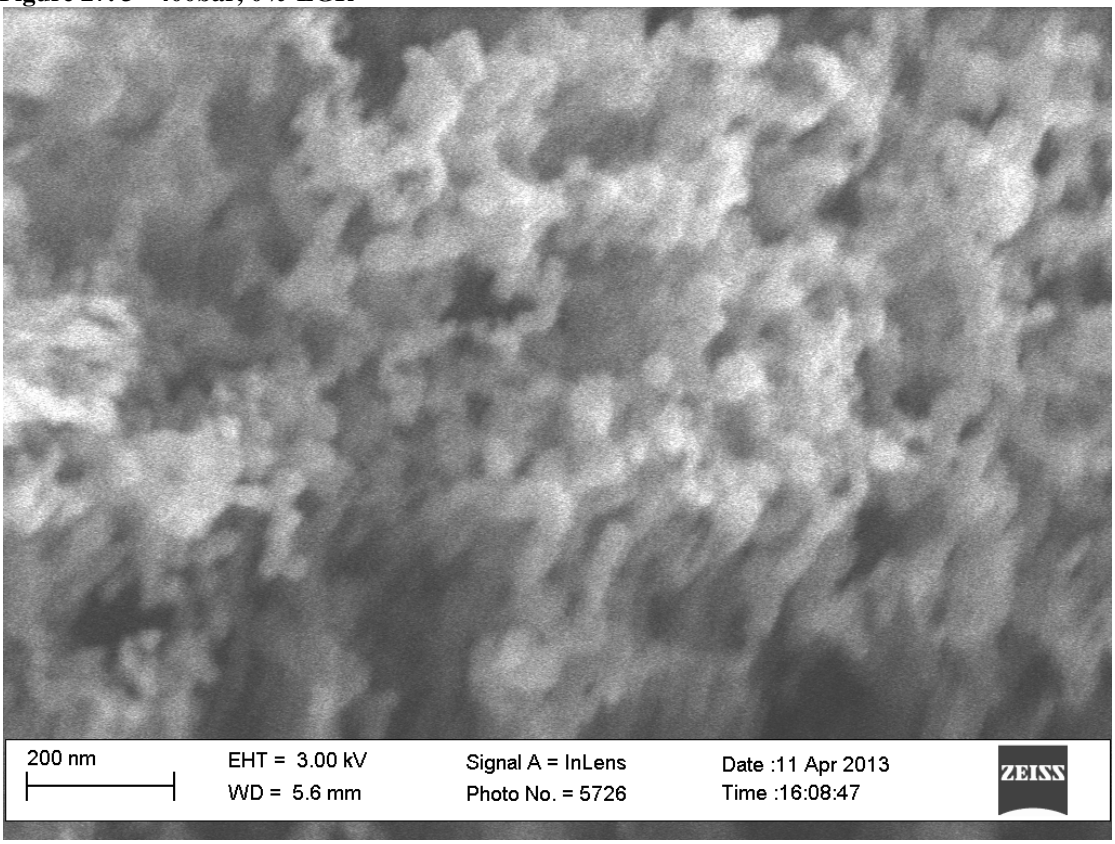

Figure 28. 4 - 550bar, 40% EGR

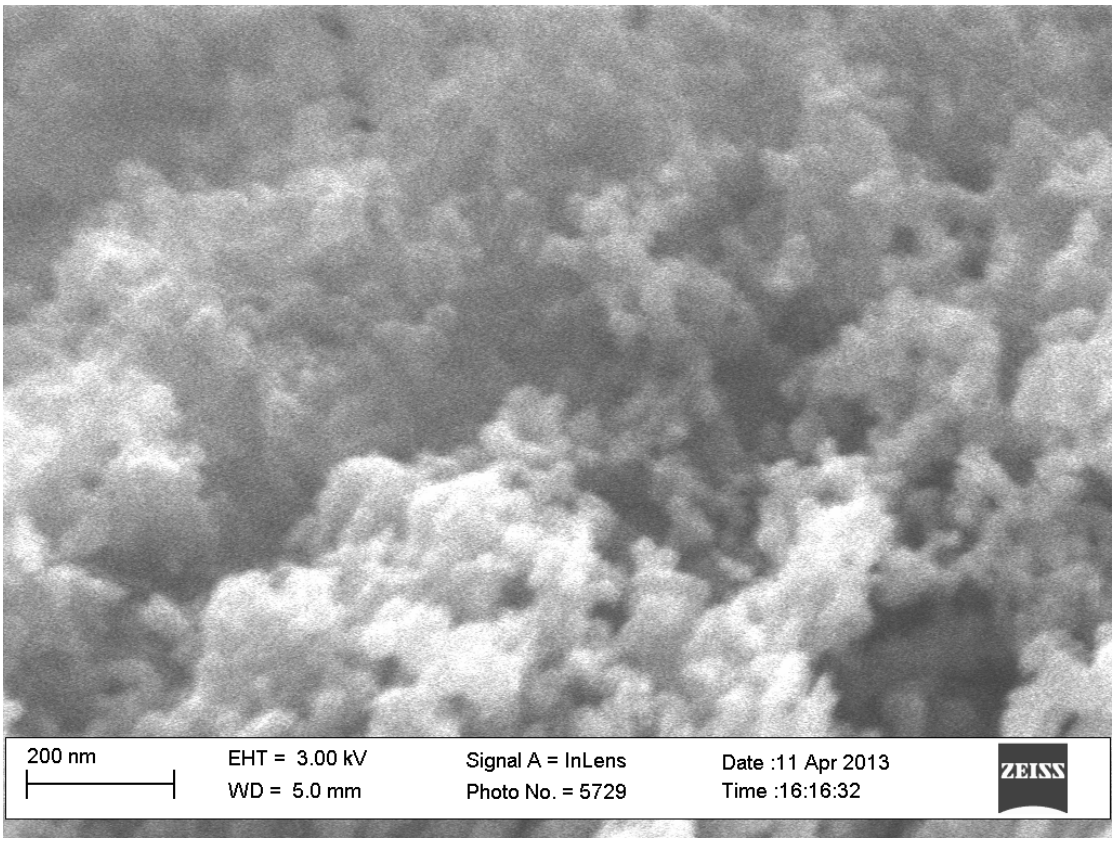

Figure 29. 5 - 400bar, 0% EGR, ash

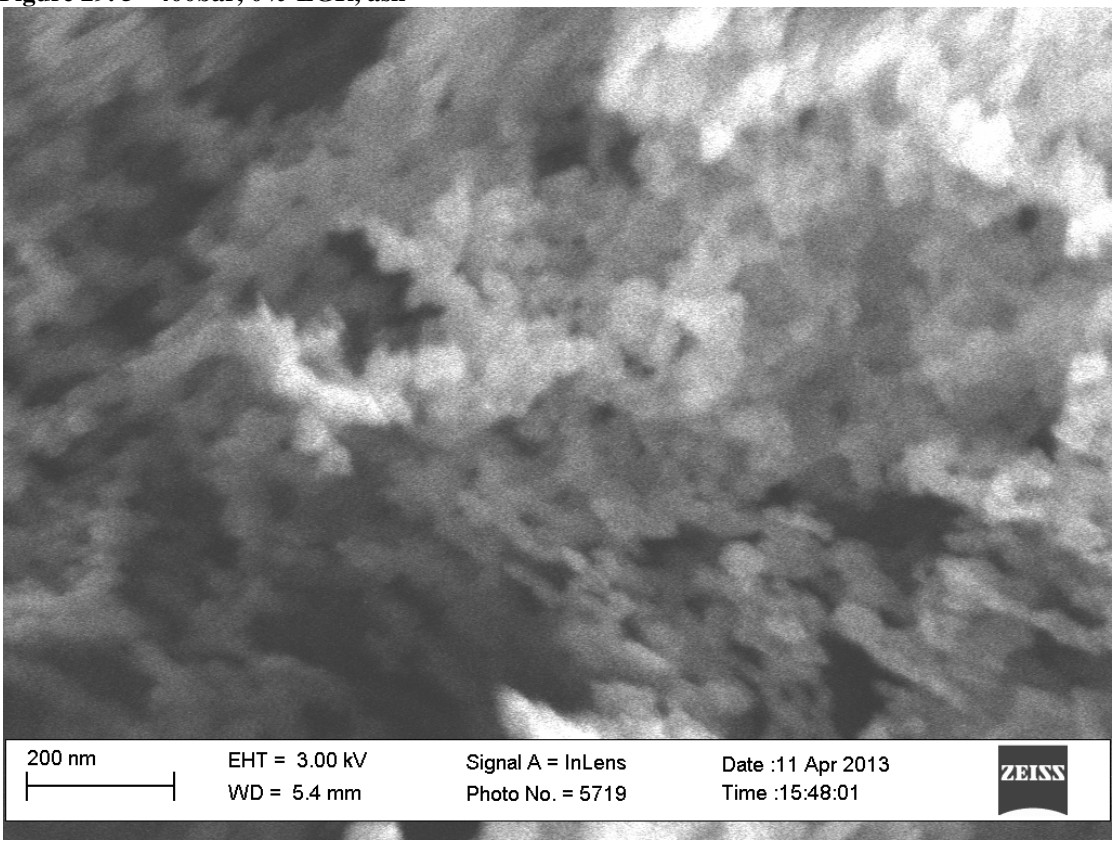

Figure 30. 6 - 600bar, 0% EGR

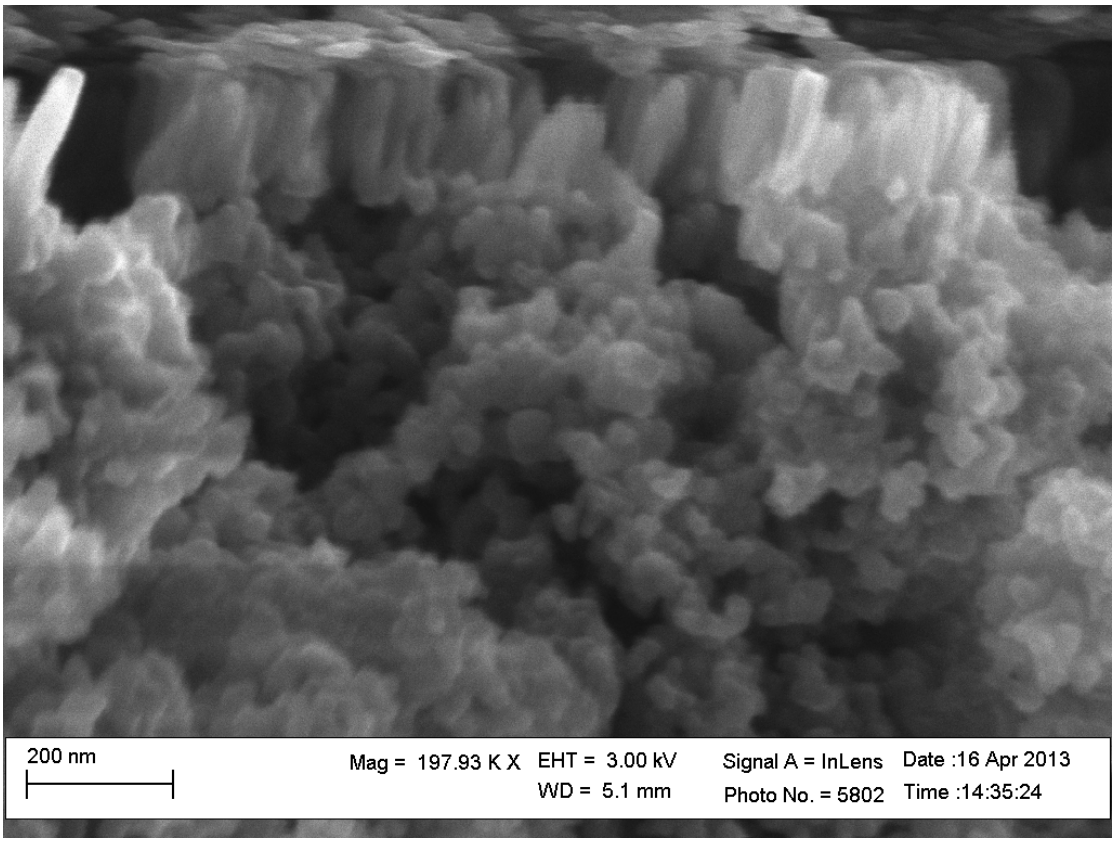

Figure 31. 7 - EGR manifold

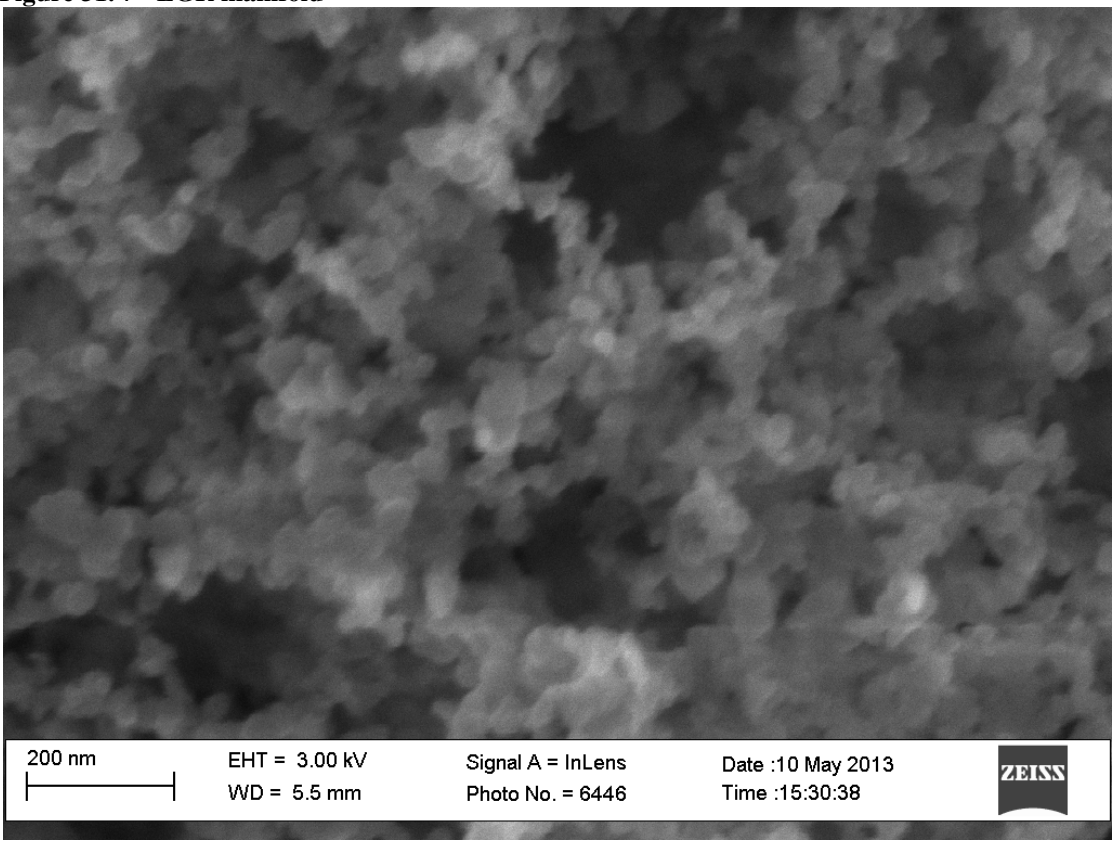

Figure 32. 8 - Normal loading